Strong margin influence on the Arctic Ocean barium cycle revealed by Pan-Arctic synthesis

Laura M. Whitmore[1], Alan M. Shiller[1], Tristan J Horner[2], Yang Xiang[3], Maureen E Auro[2], Dorothea Bauch[4], Frank Dehairs[5], Phoebe J. Lam[6], JINGXUAN LI[2], Maria Teresa Maldonado[7], Chantal Mears[8], Robert Newton[9], Angelica Pasqualini[9], Hélène Planquette[10], Robert Rember[11], and Helmuth Thomas[12]

[1]University of Southern Mississippi
[2]Woods Hole Oceanographic Institution
[3]Department of Ocean Sciences, University of California at Santa Cruz
[4]University Kiel
[5]Vrije Universiteit Brussel (AMGC)
[6]University of California, Santa Cruz
[7]University of British Columbia
[8]Institute for Coastal Research, Helmholtz Centre Geesthacht
[9]Columbia University
[10]French National Centre for Scientific Research (CNRS)
[11]International Arctic Research Center, University of Alaska Fairbanks
[12]Institute for Coastal Research, Helmholtz Center Geesthacht

November 24, 2022

Abstract

What controls the distribution of barium (Ba) in the oceans? Answers to this question have been sought since early studies revealed relationships between particulate Ba (pBa) and POC and dissolved Ba (dBa) and silicate, suggesting applications for Ba as a paleoproductivity tracer and as a tracer of modern ocean circulation. Herein, we investigated the Arctic Ocean Ba cycle through a one-of-a-kind data set containing dissolved (dBa), particulate (pBa), and stable isotope Ba (δ138Ba) data from four Arctic GEOTRACES expeditions conducted in 2015. We hypothesized that margins would be a substantial source of Ba to the Arctic Ocean water column. The dBa, pBa, and δ138Ba distributions all suggest significant modification of inflowing Pacific seawater over the shelves, and the dBa mass balance implies that ˜50% of the dBa inventory (upper 500 m of the Arctic water column) is not supplied by conservatively advected inputs. Calculated areal dBa fluxes are up to 10 µmol m-2 d-1 on the margin, which is comparable to fluxes described in other regions. Applying this approach to dBa data from the 1994 Arctic Ocean Survey yields similar results. Surprisingly, the Canadian Arctic Archipelago did not appear to have a similar margin source; rather, the dBa distribution in this section is consistent with mixing of Arctic Ocean-derived waters and Baffin-bay derived waters. Although we lack enough information to identify the specifics of the shelf sediment Ba source, we suspect that a terrigenous source (e.g., submarine groundwater discharge or fluvial particles) is an important contributor

Strong margin influence on the Arctic Ocean barium cycle revealed by Pan-Arctic synthesis

Laura M. Whitmore[1]*, Alan M. Shiller[1*], Tristan J. Horner[2], Yang Xiang[3], Maureen E. Auro[2], Dorothea Bauch[4], Frank Dehairs[5], Phoebe J. Lam[3], Jingxuan Li[6], Maria T. Maldonado[6], Chantal Mears[7], Robert Newton[8], Angelica Pasqualini[9], Hélène Planquette[10], Robert Rember[11], Helmuth Thomas[7]

[1]School of Ocean Science and Engineering, University of Southern Mississippi, Stennis Space Center, Mississippi, USA; [2]NIRVANA Laboratories, Woods Hole Oceanographic Institution, Woods Hole, MA 02543, USA; [3]Department of Ocean Sciences, University of California, Santa Cruz, CA 95064 USA; [4]GEOMAR Helmholtz Centre for Ocean Research, Kiel, Germany; [5]Analytical, Environmental and Geochemistry, Vrije Universiteit Brussel, 1050 Brussels, Belgium; [6]Earth Ocean & Atmospheric Sciences, University of British Columbia, Vancouver, BC, Canada**;** [7]Institute for Coastal Research, Helmholtz Centre Geesthacht, Geesthacht, Germany; [8]Lamont-Doherty Earth Observatory, Columbia University; [9]Department of Earth and Environmental Engineering, Columbia University, New York, NY, USA; [10] Univ Brest, CNRS, IRD, Ifremer, LEMAR, F-29280 Plouzane, France; [11]International Arctic Research Center, University of Alaska Fairbanks, Fairbanks, Alaska 99775, USA

Corresponding author: Laura M. Whitmore (lmwhitmore@alaska.edu) and Alan M. Shiller (alan.shiller@usm.edu)

Key Points:

- A mass balance approach indicates margin sources of barium account for ~50% of the budget.
- North American Arctic Ocean samples exhibit inverted Ba isotope profiles, though still fall on the global array.
- Particle supply from the shelves and dissolution in the deep North American Arctic Ocean is a likely source of dissolved barium.

Key words: GEOTRACES, barium isotopes, geochemical cycles, climate, continental shelves

Abstract

What controls the distribution of barium (Ba) in the oceans? Answers to this question have been sought since early studies revealed relationships between particulate Ba (pBa) and POC and dissolved Ba (dBa) and silicate, suggesting applications for Ba as a paleoproductivity tracer and as a tracer of modern ocean circulation. Herein, we investigated the Arctic Ocean Ba cycle through a one-of-a-kind data set containing dissolved (dBa), particulate (pBa), and stable isotope Ba (δ^{138}Ba) data from four Arctic GEOTRACES expeditions conducted in 2015. We hypothesized that margins would be a substantial source of Ba to the Arctic Ocean water column. The dBa, pBa, and δ^{138}Ba distributions all suggest significant modification of inflowing Pacific seawater over the shelves, and the dBa mass balance implies that ~50% of the dBa inventory (upper 500 m of the Arctic water column) is not supplied by conservatively advected inputs. Calculated areal dBa fluxes are up to 10 µmol m^{-2} d^{-1} on the margin, which is comparable to fluxes described in other regions. Applying this approach to dBa data from the 1994 Arctic Ocean Survey yields similar results. Surprisingly, the Canadian Arctic Archipelago did not appear to have a similar margin source; rather, the dBa distribution in this section is consistent with mixing of Arctic Ocean-derived waters and Baffin-bay derived waters. Although we lack enough information to identify the specifics of the shelf sediment Ba source, we suspect that a terrigenous source (e.g., submarine groundwater discharge or fluvial particles) is an important contributor.

Plain Language Summary

We investigated the barium cycle in the Arctic Ocean. The oceanic barium cycle is supported by the interplay of seawater mixing, river inputs, sediment inputs, and particle formation and export from the water column. We determined that the distribution of dissolved barium in the upper 500 m of the Arctic Ocean is largely set by a shelf sediment source; this is newly described, as previous literature assumed rivers and seawater mixing were the predominant contributors to the distribution. This discovery fits in with recent findings that the shelf sediments are a major source of radium and other trace metals to the surface Arctic Ocean. This is important to consider as the warming climate continues to erode Arctic ice cover (sea ice or glacial).

Monitoring the relative sources of Ba to the water column can help define how warming impacts Arctic Ocean biogeochemistry.

1 Introduction

The Arctic sits at the forefront of global change, and we have already observed the manifestation of anthropogenic effects in the region (Wassmann et al., 2011). The Arctic Ocean is a particularly climate-relevant ocean basin due to the impact is has on the formation of North Atlantic Deep Water (NADW), which is a driver of the Atlantic Meridional Overturning Circulation (AMOC), and also due its impact on planetary albedo through sea-ice coverage. The distribution of heat and freshwater within the Arctic Ocean, which is determined by the relative contributions of different source waters, modulates deep water formation, sea-ice extent, and ecosystem functioning.

Geochemical tracers have played a central role in unraveling the distributions of water types within the Arctic Ocean, though non-conservative processes have often complicated interpretations (e.g., Whitmore et al., 2020 and references therein). In the case of barium (Ba), an improved understanding of the sources, sinks, and internal processes influencing Ba distribution is required to evaluate its use as a tracer. The global vertical Ba distribution has evidence of depletion in the surface and increases with depth; it's nutrient-like profile has often been ascribed to particle formation in surface and mesopelagic depths and dissolution in the deep basins (Bishop, 1988; Chan et al., 1977; Chung, 1980). The stable isotope composition of dBa (δ^{138}Ba) is another means to assess the relative influence of sources and internal cycling on the dBa distribution. Oceanic dissolved δ^{138}Ba profiles are typically enriched in isotopically heavy Ba at the surface and depleted at depth. Such a profile is generally compatible with removal of isotopically light Ba in the surface—presumably into barite—and regeneration at depth; however, recent literature has unveiled the importance of regional circulation on the δ^{138}Ba distribution (e.g., Bates et al., 2017; Horner et al., 2015; Hsieh & Henderson, 2017).

The distribution of dissolved Ba (dBa) in the Arctic Ocean is unique in that higher concentrations of dBa can be observed in the surface (Guay & Falkner, 1997; Guay et al., 2009), which possibly highlights the importance of circulation on the Ba distribution in this region. To our benefit, dissolved barium (dBa) has a history of use within the Arctic Ocean, mainly as a

potential tracer of fluvial input (e.g., Abrahamsen et al., 2009; Guay et al., 2009; Guay & Falkner, 1997; Taylor et al., 2003), which offers an opportunity to assess its distribution through time in the context of a changing Arctic.

Roughly 10% of the world's river discharge, most of it in two major North American and four major Asian river systems, enters the Arctic marine system (Milliman & Farnsworth, 2013). Freshwater from rivers, among precipitation and low salinity Pacific waters, contributes to estuarine-like characteristics in the Arctic Ocean basin; that is, surface waters are relatively fresh and there is a strong halocline. High concentrations of dBa in Arctic rivers relative to seawater, and in North American rivers relative to Eurasian rivers, have prompted the use of Ba as a tracer of continental freshwater (Guay & Falkner, 1997).

A number of studies have followed up on this suggestion to further assess the viability of Ba as a fluvial source tracer in the Arctic Ocean (Abrahamsen et al., 2009; Alkire et al., 2015; Guay et al., 2009; Roeske et al., 2012a). Such work has suggested that much of the Arctic Ocean riverine component is derived from Eurasian rivers; however, these studies also acknowledge that non-conservative processes, such as particle formation, may influence dBa distribution. Nonetheless, few studies have been able to quantify the non-conservative behavior of dBa in the Arctic (Hendry et al., 2018; Roeske et al., 2012a; Taylor et al., 2003; Thomas et al., 2011), which limits its utility to a predominantly qualitative descriptor of freshwater sources. Thomas et al. (2011) and Hendry et al. (2018) assessed dBa distributions in the Amundsen Gulf and north of Svalbard, respectively. These studies came to similar conclusions: that biological Ba precipitation seasonally influences Ba in surface waters (i.e., < 50 m). Thus, in this context, one goal of our work is to expand the scope of previous studies to a pan-Arctic perspective to assess non-conservative Ba sources and sinks in the Arctic marine system.

Internal cycling of Ba has oft complicated our understanding of Ba distributions. Following an empirical correlation between barite sinking flux and particulate organic carbon export flux (Dymond et al., 1992), pBa observations, in both the water column and sediments, has been applied as a proxy for productivity and carbon export (e.g., Dehairs et al., 1980, 1997; Dymond et al., 1992; Eagle et al., 2003). However, the mechanisms driving the barite-export relationship remain unclear (Cardinal et al., 2005; Chow & Goldberg, 1960; Dehairs et al., 1980; Ganeshram et al., 2003; Martinez-Ruiz et al., 2019), which makes application of the methodology empirical rather than mechanistic. In the central Arctic Ocean, productivity is low

relative to other ocean basins and modern measurements of export are limited (Honjo et al., 2010 and references therein; Nöthig et al., 2020). Thus, examining the pBa distribution in the Arctic Ocean may shed light both on processes affecting the dBa distribution as well as the potential to apply modern and paleoceanographic Ba proxies for productivity and export.

In this study we ask the question: *what controls the Ba distribution in the Arctic Ocean?* Under the traditional framework the dBa cycle is supported by circulation, particulate Ba (pBa) formation and dissolution, and inputs from the seafloor (Carter et al., 2020; Dickens et al., 2003; Hendry et al., 2018; Jacquet et al., 2005). In the Arctic Ocean, circulation has largely been expected to set the dBa distribution with seawater inflow and river input as the predominant sources of dBa (e.g., Guay et al., 2009; Taylor et al., 2003). However, in this region, sea ice dynamics and margin influences must also be considered among potential non-conservative sources and sinks. Margins have been identified as an important source of trace elements to the ocean (Jeandel et al., 2011; Lam & Bishop, 2008; Mayfield et al., 2021). Due to its broad continental shelves and the expected increase in margin fluxes with the decline in sea ice coverage (Charette et al., 2016; Kipp et al., 2018), the role of Arctic Ocean margins in the Arctic Ba cycle is especially important to evaluate. We hypothesized that margin sources may contribute a significant amount of Ba to the water column. Herein, we consider 'margin sources' to include any number of Ba sources over the continental margin, such as benthic dissolution flux or submarine groundwater discharge (SGD).

To address this hypothesis we investigated the sources (seawater inflow, rivers, margins, and sea ice), internal cycling (formation and dissolution of pBa), and sinks of dBa (burial of barite and water outflow). Utilizing mass/flux balance approaches under the assumption of steady state, we quantified Ba fluxes in the Arctic Ocean. We used dissolved and particulate data from four 2015 GEOTRACES expeditions (GN01 [USA], GN02/3 [CAN], and GN04 [EU]), dissolved Ba isotope data from GN01 [USA], historical Ba data (rivers, halocline, and an extensive survey from 1994), and draw on other GEOTRACES results to ascribe the importance of each of these terms.

2 2015 Arctic GEOTRACES Sections

Four oceanographic expeditions were conducted between July and October 2015 that encompassed the North American and Eurasian sectors of the Arctic Ocean, and included shelf

areas such as the Bering Sea, Barents Sea, and Canadian Arctic Archipelago (Figure 1). The cruises were conducted within the framework of the international GEOTRACES program and mark an early effort to characterize trace elements and their isotopes in the pan-Arctic domain. Cruises departed from the United States (GN01: Aug. 9 – Oct 12, 2015), Norway (GN04: Aug. 17 – Oct. 14, 2015), and Canada (GN02 & GN03: July 10 – Aug. 20, 2015 & Sept. 4 – Oct. 1, 2015, respectively) and are referred to by their GEOTRACES cruise ID (GN0#) throughout the text.

GN01 transited through the Bering and Chukchi Seas to the North Pole and completed two transects: one in the Makarov Basin (180°W) and another in the Canada Basin (150°W). GN02 and GN03 completed surveys through the Canadian Arctic Archipelago, with a primary transect from the Canada Basin in the North American Arctic Ocean through Baffin Bay to the Labrador Sea (Figure 1a, 1b). GN02 and GN03 also conducted a high resolution cross section across Lancaster Sound (see Section 5.6). GN04 sampled a transect from the Barents Sea to the North Pole roughly along the 30°E longitudinal line (due to ice conditions, there are longitudinal variations in the transect). Additionally, GN04 completed a high resolution transect perpendicular to 135°E. Each cruise shared a crossover station and data from these stations were analyzed for quality control and intercalibration purposes (See Supplementary Text S3).

Throughout the manuscript, we will refer to the key regions as the ‘North American Arctic Ocean’, ‘central Arctic Ocean’, ‘Eurasian Arctic Ocean’ and ‘Canadian Arctic Archipelago (CAA)’. The North American and Eurasian Arctic Ocean are the North American and Eurasian sides of the Lomonosov Ridge, respectively (Figure 1c). The central Arctic Ocean is the region north of 85°N, which—during the 2015 expeditions—was influenced by Transpolar Drift waters (Charette et al., 2020; see section 2.1 for further discussion on regional hydrography).

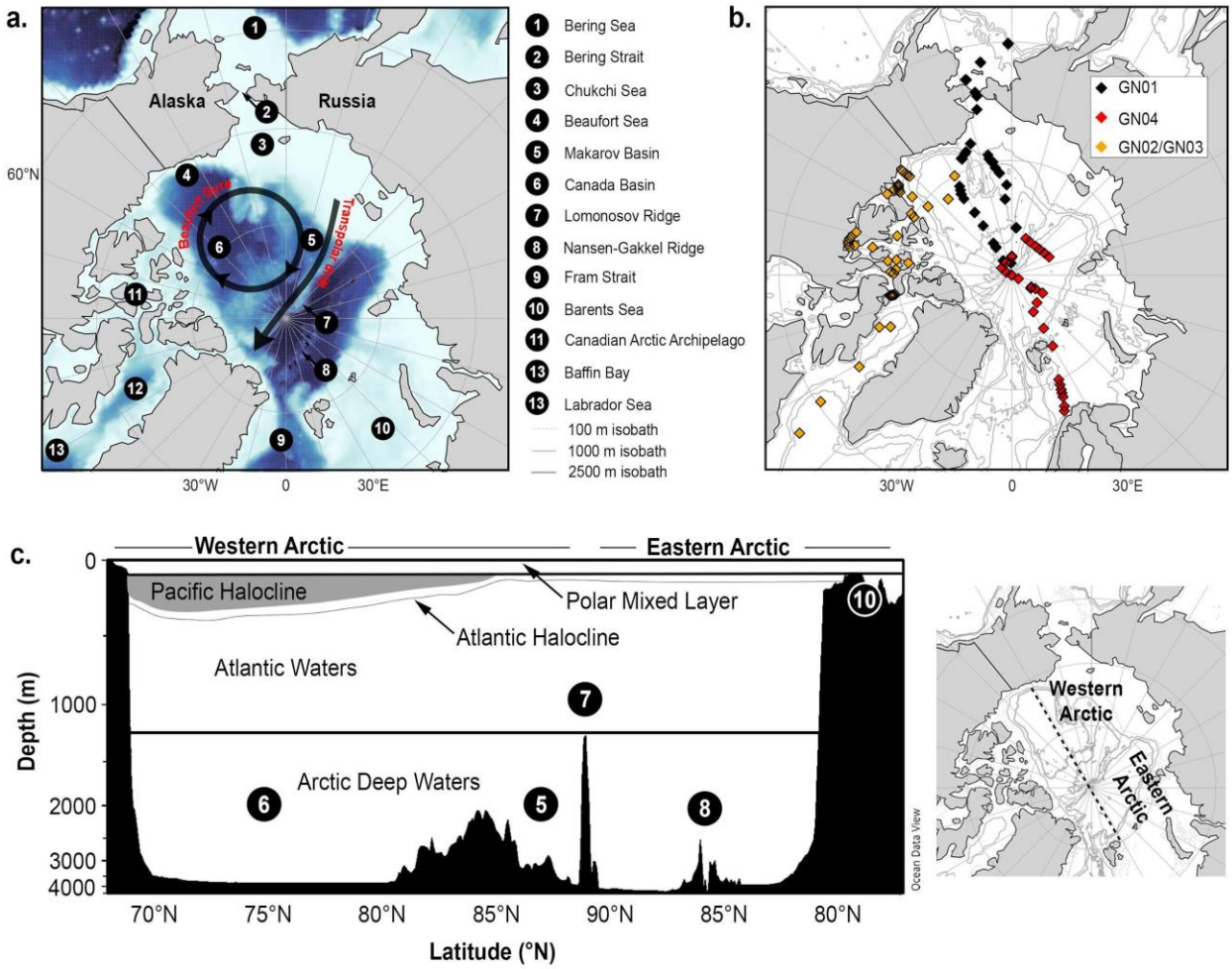

Figure 1. Regional geography, hydrography, and station map. a) Local geographic features and predominant surface circulation. b) Station map for the 2015 GEOTRACES expeditions. U.S. GEOTRACES (GN01) are black diamonds, European GEOTRACES (GN04) are red diamonds, and Canadian GEOTRACES (GN02 and GN03) are orange diamonds. c) Regional hydrographic features. Figure modified from Whitmore et al., 2019.

2.1 Regional Hydrography

Seawater enters the Arctic Ocean through the Bering Strait (Pacific-derived waters), the Fram Strait (Atlantic-derived) and the Barents Sea (Atlantic-derived). Substantial freshwater input to these regions sustain low salinity waters in the Arctic Ocean's mixed layer (Polar Mixed Layer; PML). The Arctic Ocean receives ~10% of global river discharge (e.g., McClelland et al., 2012; Milliman & Farnsworth, 2013) and is the smallest ocean basin; thus river discharge contributes to the PML basin-wide. The combination of river discharge, sea ice melt, and

Pacific-derived seawater (S ~ 32.5), yields a strong halocline expressed in the North American Arctic Ocean (Pacific Halocline; PH; Figure 1c). Pacific-derived waters undergo geochemical and physical modification due to exchange with shelf sediments, seasonal brine formation and sea ice melt, and particulate interactions and biological activity during transit on the regional shelves before entering the Arctic Ocean basins (e.g., Fransson et al., 2001; Gong & Pickart, 2016; Whitmore et al., 2019). Circulation of surface waters in the North American Arctic Ocean is set by the anticyclonic Beaufort Gyre and the Transpolar Drift (TPD); in the Eurasian Arctic Ocean, surface circulation is generally cyclonic. The TPD is a strong current that advects waters from the Chukchi, East Siberian, and Laptev seas across the central Arctic Ocean (Charette et al., 2020 and references therein).

Transformations of physical properties imparted on Pacific-derived waters such as temperature (T) and salinity (S) result in the formation of warm, fresh Pacific summer water (PSW) and cold, salty Pacific winter water (PWW) that contribute to the PH (Gong & Pickart, 2016; Weingartner et al., 1998). Warm waters in the PH are derived from waters warming over the shelf, principally summer Bering Strait Water (sBSW) or Alaska Coastal Water (ACW; Steele et al., 2004). We refer to the warm PH waters (sBSW and ACW) as 'Pacific Summer Water' (PSW) following Timmermans et al. (2014). The PH has a residence time of roughly 15 years (Kipp et al., 2019; Schlosser et al., 1999) and its distribution is sensitive to atmospheric conditions (e.g., Steele et al., 2004).

The 'Atlantic halocline' or 'lower halocline' lies directly below the PH and is likely composed of Atlantic-derived seawater that has similarly undergone modifications due to physical or biogeochemical processes occurring over the shelves (Coachman & Barnes, 1963; Rudels et al., 2004). Circulating below the halocline are Atlantic-derived 'intermediate waters'. Two distinct Atlantic-derived water masses have been identified with residence times of 20 – 30 years (Kipp et al., 2019; Schlosser et al., 1999): Barents Sea Branch Water (BSBW) and Fram Strait Branch Water (FSBW). Barents Sea Branch Waters cross the shallow Barents Sea shelf before entering the basins through St. Anna Trough; the density of these waters increases through cooling and in the basins they circulate beneath the FSBW (Rudels, 2018). Below the intermediate waters (>1500 m), Arctic Deep Water circulates within each basin. The Lomonosov Ridge restricts flow between the Eurasian Arctic Ocean basins and the North American Arctic Ocean basins (Talley et al., 2011). In the North American Arctic Ocean, the Canada and

Makarov Basins are further divided by the Alpha-Mendeleev Ridge. As there are few outflow sites for deep waters, these waters have long residence times of ~150 to 500 years (Kipp et al., 2019; Schlosser et al., 1999; Tanhua et al., 2009). Arctic Deep Water geochemical signals may be influenced by near-slope mixing processes and brines (Bauch et al., 1995; Middag et al., 2009; Roeske et al., 2012b; Rudels & Quadfasel, 1991).

Waters exiting the Arctic Ocean leave through both the Fram Strait and the Canadian Arctic Archipelago (CAA; Rudels, 2018) and ultimately contribute to North Atlantic Deep Water formation sites. Net volume fluxes out of the Fram Strait and the CAA (via Davis Strait) are roughly equivalent (~2 Sv each; Beszczynska-Möller et al., 2011). Our accounting of Ba fluxes exiting the Arctic focuses mostly on the CAA; a detailed accounting of Ba fluxes across the Fram Strait is available in Taylor et al. (2003). All waters entering the CAA must transit through one of several relatively shallow straits (< 500 m) before entering the Labrador Sea (e.g., McLaughlin et al., 2004; Melling, 2000). Flow through the CAA is generally eastward and southward; however, the straits are wide enough for counter currents to form along the coastlines (see Section 5.6; LeBlond, 1980; McLaughlin et al., 2004). Furthermore, the region is tidally influenced and winds play a role setting the surface currents (McLaughlin et al., 2004; Peterson et al., 2012).

Similar to Pacific-derived waters that transit over shelves, seawater passing through the CAA are modified during that transit. For example, sediment exchange, biological activity, river input, and sea ice melt and formation may influence the geochemical composition of CAA waters. The estimated combined discharge of all CAA rivers is about 10% of the total river discharge into the Arctic (Alkire et al., 2017; Haine et al., 2015) which accounts for roughly 1% of waters flowing through the CAA. For this study, we focus on waters in the Parry Channel (see Section 5.7).

3 Methods

3.1 Sample Collection and Analysis

For all cruises, dBa samples were filtered and collected into acid cleaned HDPE bottles from a trace metal clean rosette following GEOTRACES protocols (Cutter et al., 2014). Specifics to each rosette can be accessed via the cruise reports (https://www.geotraces.org/category/scientific-publications/cruise-reports/). Sampling protocols

for each lab group are further detailed in the Supplementary Material (Supplementary Text S1 and Text S2). Additionally, large and small fraction (> 51 µm & 0.8 - 51 µm) particulate barium (pBa) samples were collected via McLane Research in situ pumps (WTS-LV) during the GN01 section, also following GEOTRACES protocols (Cutter et al., 2014; Xiang & Lam, 2020); total particulate concentrations were determined as the sum of large and small fractions. Total particle distributions were sampled from GO-FLO bottles during GN02, GN03, and GN04. GN01 pump casts were set up as described in Xiang & Lam (2020). GN02/GN03 GO-FLO bottles were mounted to a standard trace metal clean rosette (Cutter et al., 2014) and GN04 GO-FLOs were mounted to the Titan sampling system (De Baar et al., 2008); trace metal clean bottle sampling procedures were followed (Cutter et al., 2014; Planquette & Sherrell, 2012).

3.1.1 Dissolved Barium Concentrations

Samples from GN01 were analyzed at the Center for Trace Analysis (University of Southern Mississippi; USM; Shiller, 2019). Samples from GN02/GN03 were analysed at Vrije Universiteit Brussel (VUB) and GN04 samples were analysed at the University of Alaska, Fairbanks (UAF; Rember, 2018). All samples were analyzed by isotope dilution ICP-MS (inductively coupled plasma mass spectrometry) similar to the method of Jacquet et al. (2005). Details of each lab's methodology can be found in the supplemental information including an intercalibration comparison (Supplementary Figure S1 and S2). In general, all labs reported relative standard deviation (RSD) < 2% and results at crossover stations suggest that inter-laboratory offsets were typically < 2.5 nmol/kg (i.e., < 6% of typical sample concentrations).

3.1.2 Dissolved Barium Isotopes

Dissolved Ba isotope measurements ($\delta^{138/134}$Ba) were made on a subset of the GN01 samples at the NIRVANA Labs at Woods Hole Oceanographic Institution, including all shelf samples (n = 23), Bering Sea endmember samples (n = 4), slope samples (n = 11) and some Makarov and Canada Basin samples (n = 20). Analytical methods followed those described by Bates et al. (2017). Barium-isotopic analyses were performed using a ThermoFinnigan Neptune multiple collector ICP-MS situated at the WHOI Plasma Facility (See Supplementary Text S2 for further detail). Sample isotopic composition was solved iteratively—with additional nested

loops for isobaric corrections—and reported relative to the nearest four bracketing measurements of NIST standard reference material 3104a in delta-notation (Eqn. 1).

$$\delta^{138}Ba_{NIST} \quad (‰) = \left(\frac{{}^{138/134}Ba_{sample}}{{}^{138/134}Ba_{NIST}} - 1\right) \times 1000 \qquad \text{(Eqn. 1)}$$

All samples were analyzed between 2 and 8 times (median n = 4). Reported values represent the weighted mean of n measurements, whereby the weightings were assigned according to the inverse square of the corresponding measurement uncertainty. Uncertainties are reported as the greater of either the weighted uncertainty for n measurements (± 2 SE, standard error), or our long-term precision of ± 0.03 permil (± 2 SD, standard deviation; Horner et al., 2015). Standard reference material and precision of analyses are reported in the Supplemental Material (Table S1).

3.1.3 Particulate Barium Concentrations

Particle samples were analyzed by ICP-MS at the UCSC Plasma Analytical Facility (GN01; Lam, 2020), at UBC (GN02/GN03), and Pôle Spectrométrie Océans/LEMAR (GN04). Particulate barium concentrations were obtained via a refluxing digestion method (Cullen & Sherrell, 1999; Ohnemus et al., 2014; Planquette & Sherrell, 2012; Xiang & Lam, 2020). The digestion included refluxing of the sample with a strong acid solution at high heat (e.g., HNO_3, HF and/or HCl) followed by drying down of the acid mixture (Supplementary Text S2). Final pBa sample solutions were analyzed in low resolution. Indium (1 ppb) was used as an internal standard for ICP-MS analysis.

The lithogenic and non-lithogenic components of pBa are considered; we assume the non-lithogenic fraction represents authigenically formed barite. This fraction is determined by adjusting the observed particulate concentrations of barium and aluminum by the terrigenous Ba:Al ratio (Eqn 2; Jacquet et al., 2005). The terrigenous Ba:Al ratio (0.0015 mol:mol) was determined from upper continental crust (UCC) values reported by Rudnick & Gao (2014) as 628 µg Ba/g and 15.4 % (wt) Al_2O_3.

$$pBa_{nonlithogenic} = pBa_{obs} - \left(pAl_{obs} \times \frac{Ba_{UCC}}{Al_{UCC}}\right) \quad \text{(Eqn. 2)}$$

3.1.4 Ancillary Data

Ancillary data, such as salinity and temperature, were retrieved from public databases when possible, including BCO-DMO for GN01 (Cutter et al., 2019) and PANGAEA for GN04 (Ober et al., 2016). Water mass fractions for the Arctic Ocean basins were determined using a four-component linear mixing model. The four-component mixing model uses salinity (S), water oxygen isotopic composition (δ18O), and nitrate and phosphate to determine the fraction of Atlantic, Pacific, meteoric, or sea-ice derived waters in each sample. This method is outlined in greater detail elsewhere (Newton et al., 2013), but employs the relative differences in N:P ratio between Atlantic and Pacific water as a tracer of each water type. Using nutrients in a water mass deconvolution relies on the assumption that the ratio of those nutrients behave conservatively, recent studies have demonstrated potential for other tracers to similarly deconvolve the water column (Andersson et al., 2008; Laukert et al., 2017; Whitmore et al., 2020). However, only nutrient data was available for all samples in the upper 500 m; therefore, we utilized the nutrient approach.

3.2 Data Analysis

The three cruises cover a large area of the Arctic Ocean. Given the good inter-laboratory agreement, we combined datasets from different cruises to produce composite ocean sections covering large swathes of the Arctic Ocean. We defined two sections in the Arctic Ocean basins and one through the Canadian Arctic Archipelago. Section A includes stations in the Bering and Chukchi seas, the Makarov Basin (along the Alpha-Mendeleev Ridge) and into the Amundsen Basins (Figure 3a). Section B progresses from the Chukchi Sea shelf-break, through the Canada, Amundsen and Nansen basins and onto the Barents Sea Shelf (Figure 3b). Section C progresses from the Canada Basin, through the Canadian Arctic Archipelago, through Baffin Bay and ends south of Baffin Bay (Figure 3c). Section plots were generated using weighted-average gridding in Ocean Data View 5.1.5 (Schlitzer, 2018).

In this study, we calculated 'predicted' dissolved barium (dBa_{pred}) to investigate the conservative behavior of dBa and $\delta^{138}Ba$. Predicted dBa was calculated following Equation 3.

$$dBa_{pred} = dBa_{met}f_{met} + dBa_{ice}f_{ice} + dBa_{pac}f_{pac} + dBa_{atl}f_{atl} \quad \text{(Eqn. 3)}$$

The four components identified in the subscripts of Equation 3 are: meteoric (*met*, representative of riverine component and precipitation), sea ice melt/formation (*ice*), Pacific-derived waters (*pac*) and Atlantic-derived waters (*atl*). The dBa of each endmember is weighted by the fraction (*f*) of the component to determine the predicted concentration of dBa (dBa_{pred}) in each sample. Barium endmembers for these components are described in Section 3.2.1 (Table 1) and the fractions were determined using a linear water mass deconvolution (Section 3.1.4).

The $Ba_{anomaly}$ (Equation 4) is the deviation of dBa from the predicted distributions. An anomaly value of 0 indicates that measured dBa matches predictions, implying conservative behavior. Barium excesses ($Ba_{anomaly} > 0$) indicate observed dBa concentrations higher than predicted, suggesting an additional source of Ba not accounted for in the mixing model. Deficits ($Ba_{anomaly} < 0$) indicate dBa removal relative to conservative behaviour.

$$Ba_{anomaly} = dBa_{obs} - dBa_{pred} \quad \text{(Eqn. 4)}$$

Saturation state, and saturation indices, are indicative of whether or not an ion is undersaturated, saturated, or supersaturated relative to the solid phase. The surface ocean is generally undersaturated in respect to barite ($BaSO_4$; Monnin et al., 1999). Theoretical saturation occurs when the saturation state (Ω_{barite}) equals 1; however, realistically, Ba is at saturation at values near 1 (Monnin et al., 1999). Spontaneous nucleation of barite does not occur in solutions with $\Omega_{barite} < 8$ (Horner & Crockford, 2021; Nancollas & Purdie, 1963) and the precipitation of barite is unlikely in the absence of organic matter-Ba interactions (Deng et al., 2019). Saturation state in seawater of barium with respect to barite accounting for temperature and pressure was parameterized by Rushdi et al. (2000). Barite saturation state is formulated (Eqn. 5) as the ratio

of the ion activity product (of Ba and SO_4) and the solubility product constant (K_{sp}; (T. Horner & Crockford, 2021; Millero, 1982; Monnin et al., 1999; Rushdi et al., 2000).

$$\Omega_{barite} = \frac{\{Ba\}\times\{SO_4\}}{K_{sp}} \quad \text{(Eqn. 5)}$$

3.2.1 Determination of dBa endmembers

Considering the prior literature and available data, we determined a minimum, best-estimate, and maximum dBa endmember concentration for each water source in the Arctic (Table 1).

For meteoric dBa, we combine annual flow weighted means (AFWM) of the major rivers to determine an Arctic-wide estimate as well as consider the effects of estuarine processes. An average of the AFWMs from the seven major rivers represents our maximum estimate (190 nmol kg^{-1}; Holmes et al., 2018). Although it does not incorporate estuarine processes (i.e., addition of dBa through desorption from particles), it equally weights the contribution of each river to the central basin. North American river water (> 300 nmol kg^{-1}) is mainly diverted eastward toward the CAA and thus has less overall impact on the central Arctic than Eurasian Rivers (Guay & Falkner, 1997); thus, the mean of all AFWMs would bias the river Ba estimate high. Our "best-guess" estimate (130 nmol kg^{-1}) is from Guay et al. (2009) and considers both the AFWMs and previous estimates of the effective river endmember (i.e., includes estuarine processes). Our minimum estimate is an average of Eurasian river AFWMs; this is low because it does not include estuarine processes or any influence from North American rivers (Guay & Falkner, 1998; Kipp et al., 2020a).

We consider Station 4 from GN01 in the Bering Strait a representative Pacific Endmember (dBa_{pac}); dBa at the Bering Strait was 56 ± 1 nmol kg^{-1}. We recognize that Pacific derived waters have passed over the shallow Bering Sea shelf before reaching this point and compare this value to GN01 Station 1, on the slope of the Bering Sea (the Pacific-most station sampled). At GN01 Station 1 we observed dBa between 38.7 and 61.1 nmol kg^{-1} in the upper 100 m. The Bering Strait average agrees with the 54 ± 5 nmol kg^{-1} reported "Pacific Endmember" by Guay et al. (2009). Note, dBa in the Bering Strait has been reported at higher concentrations (e.g., near bottom dBa > 100 nmol kg^{-1}; Falkner et al., 1994). However, the GN01 Station 1 profile does not exceed ~70 nmol kg^{-1} in the upper 300 m and Bering Sea basin and Gulf of

Alaska surface dBa observations are ~50-60 nmol kg^{-1} (Yamamoto-Kawai et al., 2010). Thus, we attribute high observations of dBa on the shelves to sources of Ba to the shelf region (e.g., rivers, shelf sediments, internal cycling).

No seawater entering the Arctic Ocean at the Fram Strait or Barents Sea gate-ways were sampled in this set of cruises. However, we approximate the Atlantic seawater endmember as the average Eurasian Arctic Ocean basin samples between 20 and 2000 m (41.6 ± 3.7 nmol kg^{-1}). Although not directly from North Atlantic samples, this estimate supports the application of a dBa_{Atl} endmember of 42 ± 3 nmol kg^{-1} as determined from and used in previous literature (Guay et al., 2009; Le Roy et al., 2018; Roeske et al., 2012a).

Sea ice may be a source of Ba through sequestration of Ba into the sea-ice complex and release to the water column. In smaller regions, this process could be net zero in consideration of the entire water column (Thomas et al., 2011). However, in consideration of the Arctic Ocean basins we must consider the possibility that the sea-ice formed over the shelves and either melted or released brines over the basins. Importantly, the magnitude of this source and role of sea ice formation distributing dBa in the water column remains unclear (Hendry et al., 2018; Hoppema et al., 2010; Marsay et al., 2018). Although atmospheric deposition of Ba is small; accumulation in the snow and sea ice is a possibility. The sea ice endmember (dBa_{ice}) is estimated as the mean of sea-ice Ba concentrations collected during the GN01 expedition (Marsay et al., 2018). The minimum and maximum sea-ice estimates are set at plus or minus one standard deviation of the sea-ice samples.

Table 1. Dissolved Ba endmember estimates (nmol kg^{-1}).

	Minimum	**Best Estimate**	**Maximum**
dBa_{met}	90	130[1]	190
dBa_{SIM}[2]	2	6.5	11
dBa_{Pac}	55	56	57
dBa_{Atl}[1]	39	42	45

[1]Guay et al., 2009; [2]Marsay et al., 2018

4 Results

4.1 Dissolved Barium Distribution

Dissolved Ba profiles in the North American Arctic Ocean were atypical of global ocean profiles. Contrary to the nutrient-like profiles of the Atlantic and Pacific where dBa is low in the surface and increases with depth (Chan et al., 1976), we observed high concentrations of dBa (> 60 nmol kg^{-1}) in surface waters (0 - ~ 350 m; σ_θ < 27 kg m^{-3}; Figures 2, 3) in the North American Arctic Ocean, a decrease in dBa at intermediate depths (~350 – 2000 m), and an increase in deep waters (>2000 m). Comparatively, Eurasian Arctic Ocean, Baffin Bay, and Lancaster Sound dBa profiles were similar to global ocean distributions. Deep water dBa concentrations in the Eurasian Arctic Ocean do not increase to concentrations as high as those observed in deep waters of the Atlantic or Pacific (Bates et al., 2017; Hsieh & Henderson, 2017; Schlitzer et al., 2018; See Supplemental Figure S3).

Samples collected in the Chukchi and Bering Seas have a large range in dBa (11.9 – 84.5 nmol kg^{-1}; Figure 3). The extremes of this range are at one station (Station 2) influenced by a strong vertical gradient in dBa. Other shelf stations do not have as strong of a vertical gradient in dBa and are generally well mixed (Figure 4). Comparatively, the Barents Sea shelf has more classical profiles with low dBa (~32 - 40 nmol kg^{-1}) in the surface 100 m, and increasing below that to roughly 42-43 nmol kg^{-1}. The CAA shelf (through the Parry Channel) is typified by concentrations 50 and 65 nmol kg^{-1}.

Concentrations of dBa in the PML (defined at the depths where the change in density per meter is ≥ 0.1 kg m^{-2}) ranged between 39.0 – 69.3 nmol kg^{-1}, concentrations less than 53.1 nmol kg^{-1} are only observed in the Eurasian Arctic Ocean basins. Barium was slightly supersaturated with respect to barite (Ω_{barite} ~ 1.5) in the North American Arctic Ocean PML, but undersaturated in the Eurasian Arctic Ocean PML. Barite was also undersaturated or near saturation in the Baffin Bay mixed layer and the Labrador Sea mixed layer but was slightly saturated or near saturation through the Parry Channel. PML waters are influenced by advection of Pacific-derived waters, riverine input, shelf modification, and sea ice formation or melt (Carmack et al., 2016; Kipp et al., 2018). The influence of sea ice melt on PML waters was evident in the marginal ice

zone (GN01 Stations 8 – 19); surface dBa concentrations decreased where the fraction of sea ice melt increased (Pearson's R = -0.9 for stations 8 – 19 compared to R = -0.4 for Stations 8 – 65). Low concentrations of dBa were observed in sea ice sampled during this expedition (Marsay et al., 2018); thus, the melting of sea ice should dilute surface dBa.

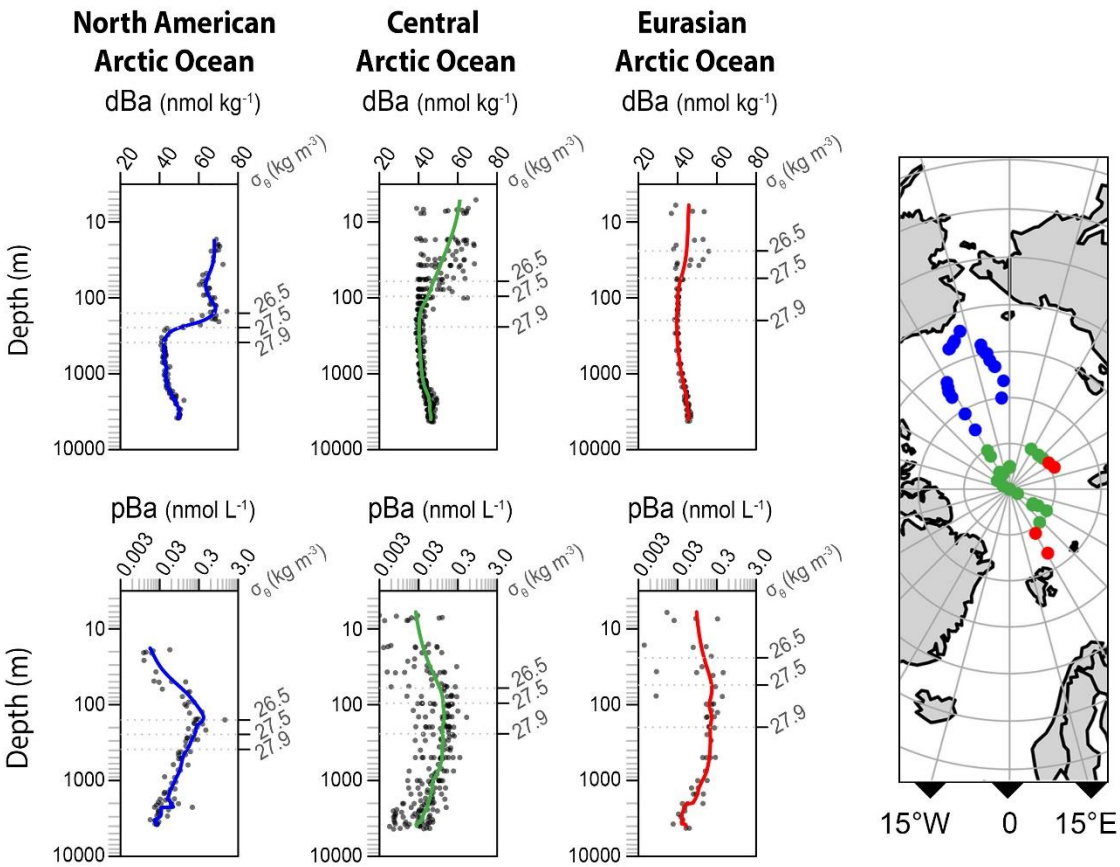

Figure 2. Mean profiles of dissolved and Particulate Ba in the North American, central, and Eurasian Arctic Ocean. Data used for mean profile come from the locations indicated in the map where the North American Arctic Ocean is blue, the central Arctic Ocean is green, and the Eurasian Arctic Ocean is red. Approximate depth of relevant water masses are indicated by their corresponding potential density (σ_θ): 26.5 kg m^{-3} is Pacific Winter Water; 27.5 kg m^{-3} is the Atlantic Halocline; 26.5 kg m^{-3} is the Atlantic Layer. Notably, PWW's are only observed in the North American Arctic Ocean, which is evidenced by the maxima in both dBa and pBa at that isopycnal.

The PH is comprised of PWW and PSW (discussed in Section 2.1) The highest dBa was observed in PWW (60.9 – 74.4 nmol kg^{-1} dBa; Figure 2) and slightly lower concentrations were observed in PSW (58 – 70.7 nmol kg^{-1} dBa; Figure 2). Dissolved Ba in both of these water masses was higher than the incoming Pacific water (56 ± 1 nmol kg^{-1}). Barite was slightly above saturation in PH halocline waters (Ω_{barite} ~ 1.4). Below the halocline waters, dBa decreased due to mixing with Atlantic-derived water. In these intermediate waters, Ω_{barite} was undersaturated in both North American and Eurasian Arctic Ocean basins.

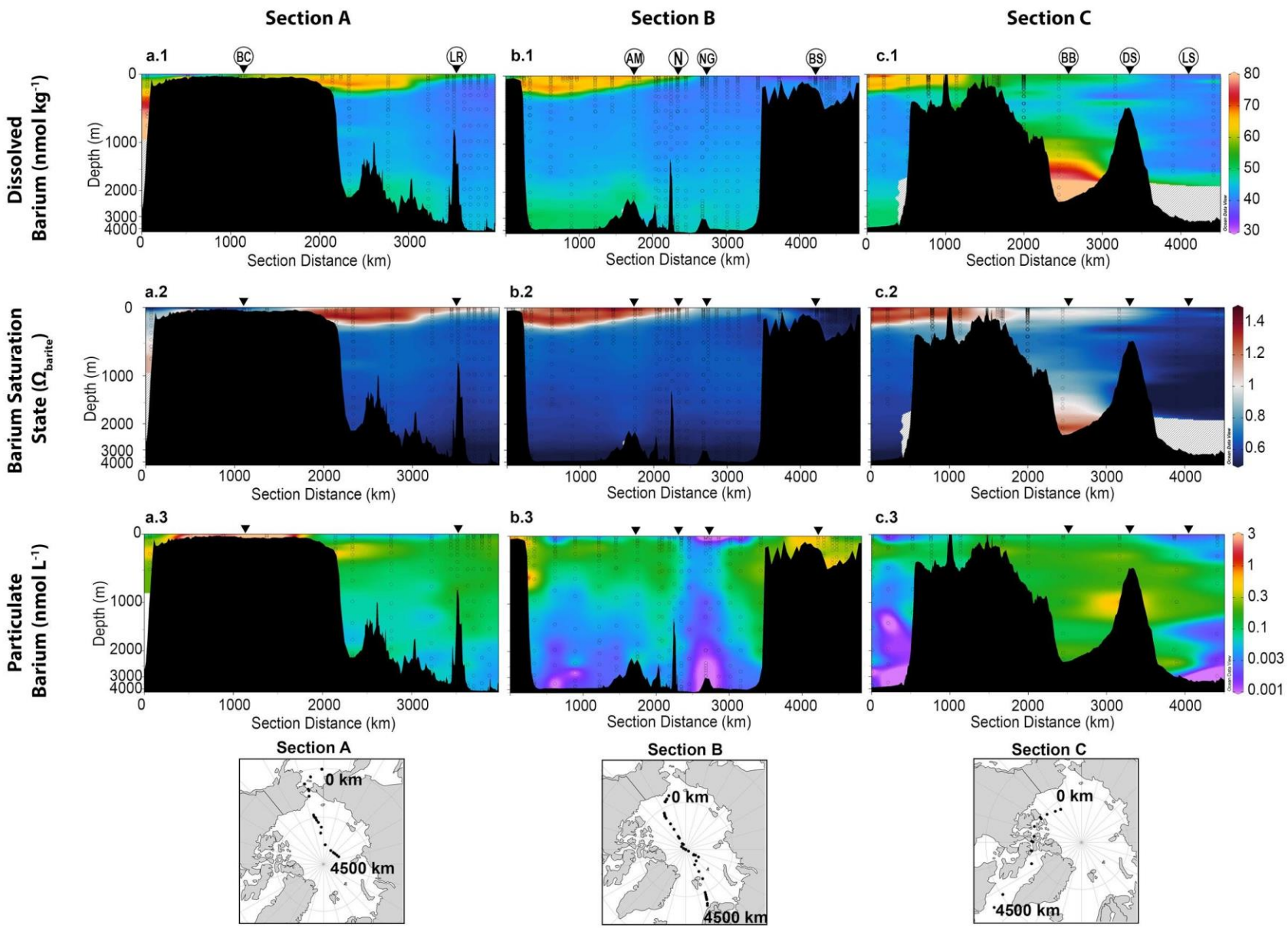
Section A
Section B
Section C
a.1
b.1
c.1
a.2
b.2
c.2
a.3
b.3
c.3
BC
LR
AM
N
NG
BS
BB
DS
LS
Dissolved Barium (nmol kg-1)
Barium Saturation State (Ωbarite)
Particulate Barium (nmol L-1)
Depth (m)
Section Distance (km)
0 km
4500 km

Figure 3. Distributions of dissolved and particulate Ba in nmol kg^{-1} and nmol L^{-1}, respectively. Each row of the figure represents a data type (i.e., same z-axis); each column represents a section (i.e., same x-axis). The rows across share the same y-axis and z-axis, viewed right of the panels. (a.1, b.1, c.1) dBa, (a.2, b.2, c.2) Barium Saturation State, (a.3, b.3, c.3) pBa for Section A, B, and C, respectively. Hashed areas indicate the background where no data was available. Location of each section is indicated in the map below each section panel. Geographic features are noted by triangles above the section plot, the labels are at the top of the dBa Section. For Section A: AM = Alpha-Mendeleev Ridge, N = North Pole, NG = Nansen-Gakkel Ridge, BS = Barents Sea. For Section B: BC = Bering & Chukchi Seas (the marker is placed at the Bering Strait), LR = Lomonosov Ridge (the LR is also in Section A, west of the North Pole). For Section C: BB = Baffin Bay, DS = Davis Strait, LS = Labrador Sea.

In comparing the deep basins (> 2000 m), dBa was highest in Baffin Bay (> 90 nmol kg^{-1}). North American Arctic Ocean deep basins (i.e., Canada and Makarov basins; Figures 3a.1, 3b.1) had average dBa of 47.9 ± 1.9 nmol kg^{-1} and Eurasian Arctic Ocean (i.e., Amundsen and Nansen) deep water had average dBa equal to 45.5 ± 1.0 nmol kg^{-1}. Even though the North American and Eurasian Arctic Ocean deep water averages are not statistically different, dBa in the North American Arctic Ocean deep basins ranged up to 52.5 nmol kg^{-1}, compared to dBa in the Eurasian Arctic Ocean, which ranged up to 47.3 nmol kg^{-1}. Thus, the North American Arctic Ocean deep waters had slightly higher dBa than the Eurasian Arctic Ocean. Baffin bay deep waters were near saturation or slightly supersaturated ($1 < \Omega_{barite} < 1.5$), all other deep basin samples were undersaturated with respect to barite.

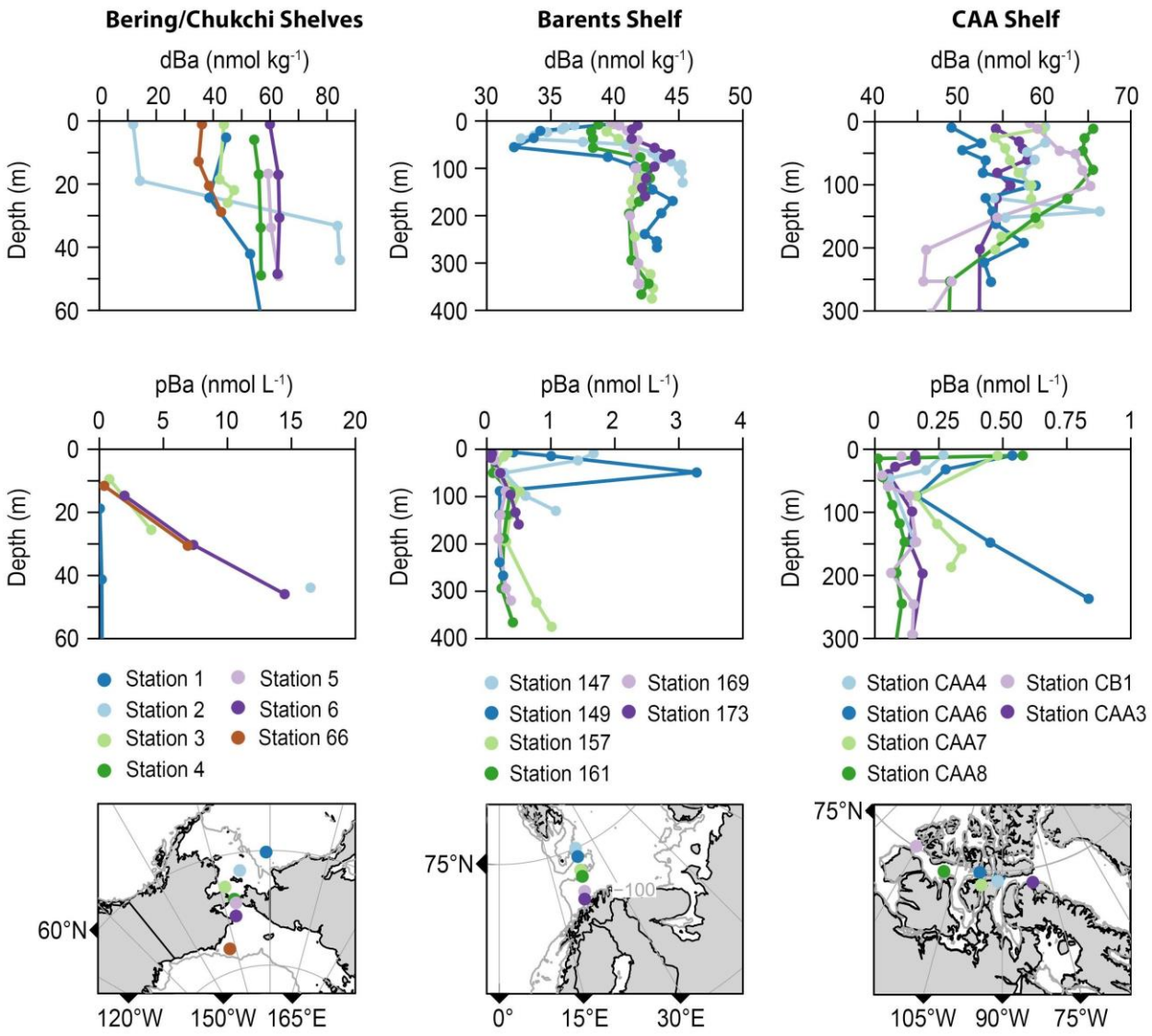

Figure 4. Shelf distribution of dBa and pBa. Left column depicts dBa and pBa profiles on the Bering and Chukchi shelves. Center column depicts dBa and pBa profiles on the Barents Sea shelf and the right column depicts dBa and pBa on the shelves of the CAA.

4.2 Particulate Barium Distribution

Arctic Ocean basins had pBa concentrations up to ~1 nmol L^{-1} (Figure 3). Maximum pBa concentrations were observed in the upper 500 m of the water column and were highest near the continental slope (Figure 3). At stations where the PH is present (North American Arctic Ocean), the pBa maximum at each station was roughly at the core of PWW (0.170 – 1.374 nmol L^{-1} pBa;

Figure 2). Comparatively, in other open ocean regions, the pBa maximum is rarely > 1 nmol L^{-1} and is typically situated near the top of the mesopelagic (roughly 200 - 1000 m; Bishop, 1988; Dehairs et al., 1997; Jacquet et al., 2005; Lam & Marchal, 2015).

Shelf concentrations of pBa are up to 16 nmol L^{-1} in the Bering and Chukchi Seas. Lithogenic particles in this region can support ~50% of the observed pBa. The highest pBa concentrations in this region are observed near the bottom (Figure 4). On the Barents Sea shelf, the maximum pBa concentration is 1.4 nmol L^{-1} and is in a surface sample at ~ 20 m depth. Some regions of the Barents Sea shelf do show an increase in pBa near the bottom – up to ~1.0 nmol L^{-1} (Figure 4). Barents Sea pBa distributions thus indicate both active surface production of barite, likely associated with productivity, and resuspension of the bottom sediments as pBa sources on the Barents Sea shelf. Indeed, the distribution of lithogenic and nonlithogenic pBa on the Barents Sea shelf supports this assessment; nearly 100% of the surface pBa (< 100 m) is nonlithogenic while 100% of bottom water pBa (> 200 m) are lithogenic.

During our sampling, pBa was < 1 nmol L^{-1} in the CAA profiles (Figures 3 and 4). Profiles in the western CAA had low pBa throughout most of the water column, excepting some surface highs (Figure 4, see stations ‘CAA8’ and ‘CB1’). Moving eastward a low pBa signal is carried through the CAA at a depth of approximately 75 m; profiles in the eastern CAA were characterized by a minimum at this depth (Figure 4). At stations east of ‘CAA8’, pBa in surface waters was predominantly nonlithogenic, whereas below the subsurface minima pBa increased to 100% lithogenic composition.

4.3 Dissolved Ba Isotope Distribution

As with dBa, the shape of the δ^{138}Ba profile in the North American Arctic Ocean differs from observations made in other ocean basins: the surface is isotopically light and δ^{138}Ba increases to a maximum near 500 m. Below 500 m, δ^{138}Ba becomes lighter and the value stabilizes below 2000 m (Figure 5a). Interestingly, despite a different vertical profile shape, the local Arctic Ocean δ^{138}Ba versus 1/dBa relationship is generally similar to the global pattern (Figure 5b).

The δ^{138}Ba value decreases across the Chukchi Shelf: the heaviest values are in the Bering Sea and δ^{138}Ba generally gets lighter moving northward into the Chukchi Sea. The lightest values are in Chukchi Sea bottom waters and in PH depth waters (50 – 150 m in the

Arctic Ocean basin; Figure 6). Comparatively, dBa generally increases from the Bering Sea into the Chukchi Sea and the PH (Figure 4). Station 66, on the Chukchi Sea shelf, which is not depicted in the Figure 6 section, does not follow this pattern and has both lower dBa and heavier δ^{138}Ba (Figures 4 and 6b). Station 2, on the Bering Sea shelf, also stands out as it has the lowest surface dBa concentrations and highest bottom dBa concentrations; δ^{138}Ba at this location is heavy in surface waters and light in bottom waters (Figures 4 and 6b). Interestingly, the surface waters at this station account for two samples that deviate from the global trend which may imply these waters have undergone substantial particulate pBa formation in the surface.

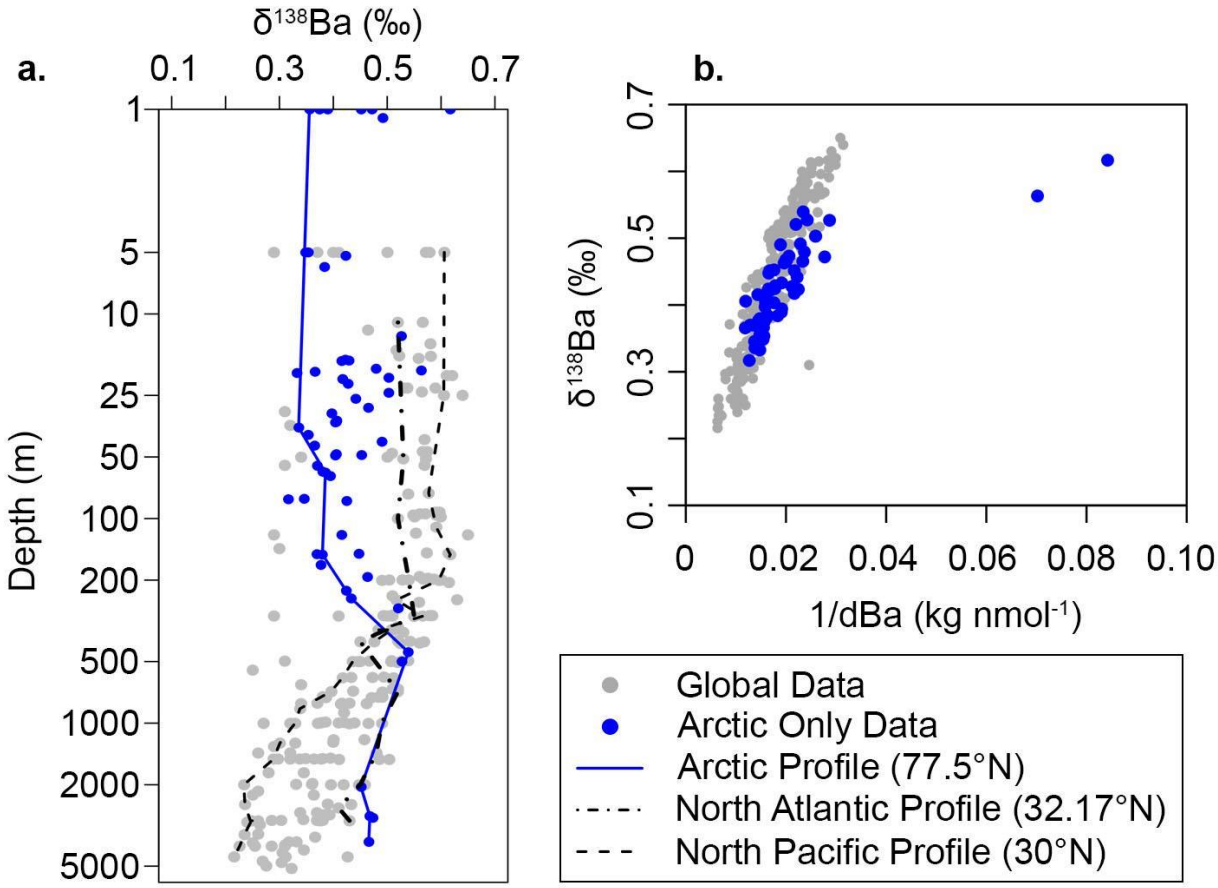

Figure 5. Arctic dissolved δ^{138}Ba distribution. a) the vertical distribution of Arctic Ocean data (blue dots) and global data (gray dots). The depth axis is logarithmically scaled to expand the surface range. Solid blue and dashed and dotted black lines are example Arctic Ocean, North

Atlantic Ocean, and North Pacific Ocean profiles, respectively. b) The dissolved δ^{138}Ba versus 1/dBa pattern.

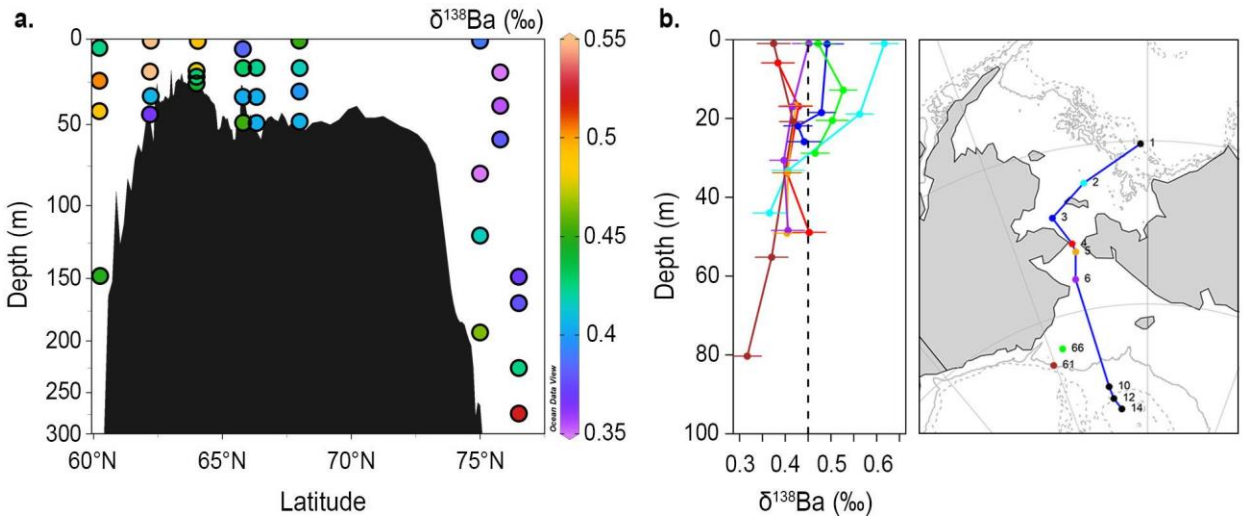

Figure 6. δ^{138}Ba distribution over the Bering and Chukchi Seas. a) The shelf section depicting dissolved δ^{138}Ba on the z-axis; the map to the right identifies the section with a blue line. b) Individual shelf station profiles, including two profiles from the Chukchi Sea that are not included in panel a. The dashed line references surface waters in the Bering Sea (Station 1).

5 Discussion

High dBa surface waters in the North American Arctic Ocean were associated with the PML and the PH (Figure 2). Importantly, Atlantic-derived waters (~42 ± 3 nmol kg^{-1}) and incoming Pacific water (~54 ± 5 nmol kg^{-1}) both have lower concentrations than what we observed in the PH (Table 1) thereby suggesting a local Arctic source of dBa. In the following sections, we evaluate Ba sources and sinks and assess their influence on the dBa distribution. Further, we discuss the role of sources and sinks on the communication of Arctic Ocean geochemical properties to the North Atlantic.

5.1 Assessing observed dBa distributions relative to predicted dBa

Our dBa distributions indicate a source of Ba to the water column that cannot be accounted for by the Pacific or Atlantic endmembers. Here, we investigate $Ba_{anomaly}$ (i.e., the

difference between observed Ba and the Ba predicted from conservative mixing; Eqn. 3 and 4) to identify where mixing of water masses can and cannot explain the observed dBa distribution. In general, we observed slight (~ -5 nmol kg^{-1}) Ba deficits in the shallow subsurface (<100 m) and moderate Ba excesses (up to 10 nmol kg^{-1}) between 100–200 m (Figure 7). These vertical patterns exhibit a strong spatial trend; the magnitude of both deficits and excesses diminishes from the North American to central Arctic Ocean, and there are essentially no dBa anomalies in the Eurasian Arctic Ocean (Figure 7).

The unequal magnitude of the surface deficit and excesses in the North American Arctic Ocean implies that vertical redistribution from the shallow formation and deeper dissolution of Ba-bearing particles cannot account for the observed $Ba_{anomaly}$ distribution.

In the central Arctic Ocean, there is a slight $Ba_{anomaly}$ deficit in surface waters. Transpolar Drift waters—which originate from the East Siberian and Laptev Seas—most strongly influence the surface 50 m and have both a shelf and riverine component (Charette et al., 2020; Kipp et al., 2018). Charette et al. (2020) reported a significant trend between dBa and the fraction of meteoric waters within the TPD. While this trend roughly extrapolates to a riverine endmember compatible with Eurasian river dBa, they noted that scatter in the trend may be indicative of shelf processes such as cycling and redistribution of dBa and/or a shelf source of dBa (Charette et al., 2020; Kipp et al., 2018; Roeske et al., 2012a). The observed dBa deficit in these TPD waters (Figure 7) suggests that, at the time TPD waters were advected from the shelves, the net effect of shelf processes on the dBa distribution in shelf surface waters was removal of dBa. This result agrees with observations in the Laptev Sea by Roeske et al. (2012a), wherein dBa and f_{met} distributions were decoupled as a result of particle formation and export.

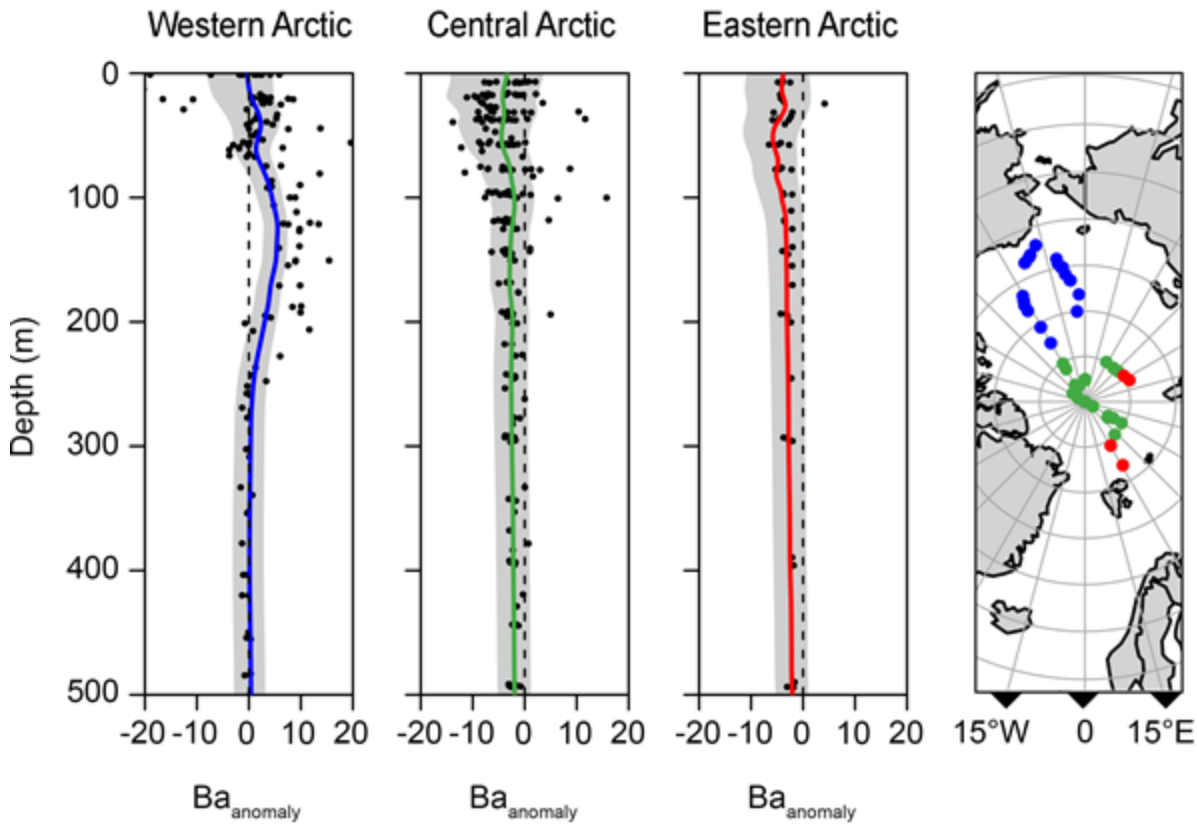

Figure 7. $Ba_{anomaly}$ (nmol kg^{-1}) for the North American, central, and Eurasian Arctic Ocean. The dashed line at $Ba_{anomaly}$ = 0 indicates the expected $Ba_{anomaly}$ for conservative behavior. The colored profile on each plot represents the mean profile for the data in the region (stations identified in the map to the right). The gray shaded region on each plot indicates the range of $Ba_{anomaly}$ if the maximum and minimum endmember estimates are used. The mean profile lines are color coded to the station map whereby blue is the North American Arctic Ocean, green is the central Arctic Ocean, and red is the Eurasian Arctic Ocean.

In the Eurasian Arctic Ocean, no $Ba_{anomaly}$ excess was observed. Although sensitive to the meteoric endmember, our best-estimate of $Ba_{anomaly}$ shows surface waters of the Eurasian Arctic Ocean clustering around zero but may have slight deficits (Figure 7). Deficits in this region are likely driven by pBa formation associated with seasonal biological activity (Hendry et al., 2018).

In comparing regions, the North American Arctic Ocean is influenced by a dBa source that is incorporated into Pacific-derived water while the Eurasian Arctic Ocean does not appear to have an equivalent source. We attribute the difference in the North American and Eurasian

Arctic Ocean $dBa_{anomaly}$ distributions to a greater amount of shelf-derived dBa from the North American Arctic Ocean shelves. However, the differences could also allude to different margin sources (i.e., authigenic vs terrigenous origin). The margin source of Ba is considered further in Section 5.4.

5.2 Barium isotopes in the upper water column: implication of a margin source

The upper water column of the Arctic Ocean basins has large lateral advective fluxes that influence dissolved and particulate distributions (e.g., Aguilar-Islas et al., 2013; Rudels, 2018). North American Arctic Ocean pBa distributions in this study support previous conclusions of advected shelf-derived particles in the PH (Aguilar-Islas et al., 2013; Kondo et al., 2016; Xiang & Lam, 2020) because concentrations of pBa are high in depths associated with PWW.

Due to such lateral inputs of dissolved and particulate material, we suspect that the δ^{138}Ba distribution in the upper water column may reflect conservative mixing of Arctic Ocean water types. However, in addition to conservative mixing, we recognize that internal cycling and margin sources could influence δ^{138}Ba distribution. Authigenic formation of pBa would leave the water column isotopically enriched in heavy Ba, whereas lateral transport of shelf particulates should not influence the dissolved Ba isotopes. As mentioned in Section 4.2, Ω_{barite} is near saturation in these waters; precipitation of Ba in the presence of organic matter nucleation sites is a possibility (Deng et al., 2019).

To test if the δ^{138}Ba distribution is supported by conservative mixing alone, we compare observed δ^{138}Ba with predicted δ^{138}Ba ($\delta^{138}Ba_{pred}$). The predicted δ^{138}Ba was determined by a linear mixing model (Eqn. 6). The denominator, dBa_{pred}, is defined in equation 3; additionally, throughout equation 6, δ^{138}Ba is identified as δ to improve readability.

$$\delta_{pred} = \frac{(\delta_{met} \times dBa_{met} \times f_{met}) + (\delta_{atlt} \times dBa_{atl} \times f_{atl}) + (\delta_{pact} \times dBa_{pac} \times f_{pac}) + (\delta_{ice} \times dBa_{ice} \times f_{ice})}{dBa_{pred}} \quad \text{(Eqn. 6)}$$

Endmember δ^{138}Ba values have not been determined for this region and endmember dBa is articulated in Section 3.2.1 (Table 1). We assessed the available literature to determine a range of reasonable endmember δ^{138}Ba for each component. Riverine δ^{138}Ba composition compiled from global observations range between ~ 0.2 ‰ and 0.46 ‰ (δ^{138}Ba ; Cao et al., 2020;

Charbonnier et al., 2018; Gou et al., 2020; T. Horner & Crockford, 2021). Similar to dBa, estuarine effects may alter the 'effective' δ^{138}Ba value (Hsieh & Henderson, 2017); however, estuarine effects on δ^{138}Ba are unconstrained.

The Pacific endmember, as a mean of previously published data from the surface 200 m of North Pacific stations, is 0.61 ± 0.02 ‰ (n = 10; Geyman et al., 2019; Hsieh & Henderson, 2017). Our study encapsulated the surface waters (< 55 m) of a station at the Bering Sea Slope and we suspect these waters may be more representative of the water entering the Arctic Ocean than the data from the northeast Pacific; at this station our data ranged from 0.42 – 0.50 ‰ (n = 3). We assessed the Atlantic endmember similarly to the Pacific; previously published surface (< 200 m) data in the North Atlantic indicate a mean δ^{138}Ba of 0.53 ± 0.03 ‰ (n = 10; Bates et al., 2017; Hsieh & Henderson, 2017).

We ran an optimization procedure in R ("optim"; R Core Team, 2018) where our cost was defined as the sum of the squared normalized residuals (SSNR). We performed a Nelder-Mead optimization, which iteratively and randomly tested possible endmembers, returning endmember values where the model-observation misfits were lowest (i.e. minimum of SSNR). In this analysis, we calculated $\delta^{138}Ba_{pred}$ by assuming that the isotopic contributions from ice were negligible since both f_{ice} in our samples and dBa_{ice} are low. Our optimized endmembers were determined as: $\delta^{138}Ba_{met}$ = 0.24 ‰, $\delta^{138}Ba_{atl}$ = 0.55 ‰, and $\delta^{138}Ba_{pac}$ = 0.40 ‰). Compared to our a priori estimates of δ^{138}Ba endmember values, the cost (SSNR) was reduced from 61 (with $\delta^{138}Ba_{pac}$ set to 0.45 ‰) to 37, indicating our optimization procedure yields a substantially improved model-observation fit.

Optimized dissolved δ^{138}Ba endmember values were within the range of our *a priori* estimates for both $\delta^{138}Ba_{atl}$ and $\delta^{138}Ba_{met}$. However, $\delta^{138}Ba_{pac}$ is lighter. To cause $\delta^{138}Ba_{pac}$ to be ≅ 0.1‰ lighter than the incoming Pacific water there is either modification to one of our endmember terms (i.e., removal of isotopically heavy Ba) or there is an additional isotopically light source term. Lateral transport of shelf-derived particles should not impact the δ^{138}Ba signal in the PH and *in situ* particle formation would leave the residual seawater heavier (von Allmen et al., 2010). Thus, conservative mixing and internal cycling cannot explain the observed δ^{138}Ba distribution and a margin source is likely. Indeed, the persistence of lighter δ^{138}Ba in shelf bottom waters and Pacific halocline waters provides support for our earlier hypothesis that there is substantial margin contribution to basin dBa.

5.3 Quantification of the dBa Budget

Our analysis of the dBa distribution (including evidence from both the dissolved $Ba_{anomaly}$ and dissolved $\delta^{138}Ba$) suggests an additional dBa source to the Arctic Ocean as well as a potential sink in surface waters. In this section we quantify the advective fluxes of dBa to determine the net magnitude of the non-conservative components. Dissolved Ba in the Arctic Ocean has advective sources from rivers, sea-ice, Pacific-derived sea water, and Atlantic-derived sea water. Dissolved barium sinks may include particle interactions and transport out of the system. At steady-state, sources balance sinks (Eqn. 7):

$$(F_{rivers} + F_{pacific} + F_{atlantic} + F_{ice} + F_{margin}) - (F_{particles} + F_{transport.out}) = 0 \text{ (Eqn . 7)}$$

where F represents the flux of dBa from sources (rivers, Pacific-derived waters, Atlantic-derived waters, ice and margin contributions) and sinks (*in situ* particle formation and circulation out of the system). Following the approach by Kipp et al. (2018), we assess the fluxes of Ba from these sources and sinks in the surface 500 m of the water column (all fluxes have units of mol y^{-1}). An issue with this approach is that it does not account for the spatial heterogeneity of the Arctic Ocean water column and treats all regions of the Arctic Ocean as homogeneous in terms of Ba distribution and residence time. Furthermore, the approach assumes steady-state and cannot identify non-steady state behavior, which is plausible given ongoing environmental change in the Arctic. However, by considering the same boundaries as Kipp et al. (2018), we can directly compare results. Our budget differs from Kipp et al. (2018) by determining the net non-conservative flux rather than the shelf-only flux. We consider the "net non-conservative" term to be the sum of F_{margin}, $-F_{particles}$, and F_{ice}, and (Eqn. 8) and it is calculated by subtracting known source fluxes from known sink fluxes.

$$F_{net-nonconservative} = F_{margin} + F_{ice} - F_{particles} = F_{rivers} + F_{pacific} + F_{atlantic} - F_{transport.out} \quad \text{(Eqn. 8)}$$

Fluxes of Ba from rivers, Pacific seawater, and Atlantic seawater were solved using the following form:

$$F_{source} = [Ba]_{source} \times Q_{source} \quad \text{(Eqn. 9)}$$

where, F_{source} represents the flux of Ba from rivers, Pacific seawater, or Atlantic seawater in mol y^{-1}. F_{source} is determined as the product of the endmember concentration of dBa in that source ($[Ba]_{source}$ as nmol m^{-3}) and the volume flux (Q) of that source into the surface 500 m (m^3 y^{-1}). The dBa endmembers for rivers, Pacific seawater, and Atlantic seawater are as described in Section 3.2.1.

We used volume fluxes derived from the literature that are largely summarized in Kipp et al. (2018). The Pacific volume flux, measured in the Bering Strait in 2011 (Woodgate et al., 2012), is $3.5 \pm 0.3 \times 10^{13}$ m^3 y^{-1}; the minimum and maximum estimates from this term are defined by the mean plus or minus one standard deviation. The Atlantic flux, a more difficult term to quantify because of the multiple pathways by which it enters the Arctic Ocean and its diffuse flow, is estimated at $2.1 \pm 0.1 \times 10^{14}$ m^3 y^{-1} (Beszczynska-Möller et al., 2012). This value is the average net flux into the Fram Strait, and thus it is not representative of the total volume entering the system. Atlantic waters entering the upper 500 m Arctic Ocean water column are a combination of Fram Strait and Barents Sea-derived waters, but likely do not account for 100% of either of those components. We follow Kipp et al. (2018) in the choice of our "best guess" Atlantic flux for consistency. However, we use only the net Fram Strait flux (plus or minus one standard deviation) as opposed to using the range of fluxes for the Fram Strait and Barents Sea branches in determining the minimum and maximum (Beszczynska-Möller et al., 2012; Rudels, 2015). The river flux term was determined from Haine et al. (2015) using data between 2000 and 2010; Q_{rivers} equals $4.2 \pm 0.4 \times 10^{12}$ m^3 y^{-1}.

The three flux terms that make up the net nonconservative term remain unconstrained: F_{margin}, $F_{particles}$ and F_{ice}. However, because of low sea ice fractions and low dBa in sea ice, the $Ba_{anomaly}$ and $\delta^{138}Ba$ endmember tests were insensitive over a range of sea ice concentrations. We thus expect F_{ice} is a minor component of the net nonconservative term. The sink from *in situ* particle formation is also assumed to be a minor component. Specifically, *in situ* formation of barite is associated with large POC particles (e.g., Lam & Marchal, 2015), possibly due to availability of surface nucleation sites (Deng et al., 2019). In the Arctic Ocean, we suspect the abundance of large POC particles (Xiang & Lam, 2020) is insufficient to result in a substantial *in*

situ pBa source ($F_{particles}$). For instance, the large (sinking) POC in Arctic surface waters is <0.5 µmol-C/kg whereas it is <2 µmol-C/kg in surface waters of other basins (Schlitzer et al., 2018). This seems to result in much higher sinking POC:$pBa_{nonlithogenic}$ in the North American Arctic (large particle range: ~90 - 90000 mol/mol; median = 2,210 mol/mol) versus other ocean basins (sediment trap range 240 and 7,200 mol/mol; median: 630 - 916 mol/mol; Francois et al., 1995; Dymond et al., 1992). This indicates that pBa cycling in the Arctic Ocean is less important than in other ocean basins. Therefore, the net nonconservative flux term is most likely dominated by F_{margin}.

To compare the 2015 data to the 1994 Arctic Ocean Survey, which replicates many of the stations in both the GN01 and GN04 transects (Supplementary Figure S4), we modified the flux terms (Eqn. 9) to be more representative of the 1990s. Haine et al. (2015) reported Q_{rivers} of 3.9 ± 0.4 × 10^{12} m^3 y^{-1} between 1980 and 2000. Woodgate et al. (2012) reported Pacific fluxes through the Bering Strait of 2.2 ± 0.3) × 10^{13} m^3 y^{-1}. Given the uncertainty in our original Atlantic flux term and the few estimates available specific to that decade, we apply the same fluxes as the 2015 mass balance. In comparing the data, there is no evidence of major changes in the dBa endmember concentrations.

To determine the flux of barium out of the system ($F_{transport.out}$) we determined an average dBa inventory for the upper 500 m of the Arctic Ocean basin by trapezoidally integrating dBa in the surface 500 m of each station where the bottom depth was > 1000 m (see Supplementary Figure S4 for a reference to the 1000 m isobath and the stations within it). Station inventories (mol m^{-2}) were averaged and then multiplied by the area of the Arctic Ocean (where the bottom depth is > 1000 m) to determine an Arctic-wide dBa inventory of (221± 25) × 10^9 mol Ba. The flux of Ba out of the system ($F_{transport.out}$) was calculated as the inventory divided by the residence time of waters in the surface 500 m. The residence time of waters in the surface 500 m is not well constrained (~1 – 30 years; Kipp et al., 2019; Schlosser et al., 1999), but in treating the surface 500 m homogeneously we use only one residence time (10 years). To determine the minimum and maximum shelf terms, we calculated the balance with the maximum source terms and minimum sink terms (minimum shelf input) and *vice versa* (maximum shelf input).

Table 2. Estimated fluxes of dBa from Arctic Ocean sources and sinks (mol y^{-1}).

	Year	Minimum Flux	Best Estimate	Maximum flux	% Of Total Sinks ("Best-Estimate")

Sinks					
Transport Out	2015	2.0×10^{10}	2.2×10^{10}	2.5×10^{10}	100
	1994	2.1×10^{10}	2.2×10^{10}	2.3×10^{10}	100
Sources					
Pacific Advection	2015	1.8×10^{9}	2.0×10^{9}	2.2×10^{9}	9
	1994	1.1×10^{9}	1.3×10^{9}	1.5×10^{9}	6
Atlantic Advection	2015	7.8×10^{9}	8.9×10^{9}	1.0×10^{10}	40
	1994	7.8×10^{9}	8.9×10^{9}	1.0×10^{10}	41
Rivers	2015	3.4×10^{8}	5.5×10^{8}	8.8×10^{8}	2
	1994	3.2×10^{8}	5.1×10^{8}	8.2×10^{8}	2
Net Non-conservative (F_{shelf}, $F_{ice.in}$, $F_{ice.out}$, $F_{particles}$)	2015	8.1×10^{9}	1.1×10^{10}	1.5×10^{10}	48
	1994	1.0×10^{10}	1.1×10^{10}	1.4×10^{10}	51
Shelf (Ba:Ra-derived)	2015	5.7×10^{9}	9.1×10^{9}	1.9×10^{10}	41
	1994	NA	NA	NA	NA

The results of the source-sink analysis reveal that around half (~52%) of the dBa transported out of the Arctic is accounted for through conservative mixing of dBa sources. This implies that net non-conservative sources are roughly 48% of the budget (Table 2). Since this approach effectively homogenizes the upper 500 m of the water column, redistribution within our box is neither a source nor sink; thus, our results indicate there must be an external source to the box.

This box model approach is sensitive to the endmember terms and fluxes. Our model is most sensitive to the residence time of waters and the inventory, which set the fluxes of barium out of the system ($F_{transport.out}$). A 15% variation in the residence time or the inventory results in roughly a 30% variation in the net non-conservative flux. The model is also sensitive to the Atlantic term, where 15% variation in the endmember or volume flux results in a 10% variation to net non-conservative flux.

Barium can have large margin fluxes, as reported in previous studies (e.g., Ho et al., 2019; Mayfield et al., 2021), and we expect a substantial part of the net-conserverative flux term to be from the margins rather than sea ice or particles. In the Arctic Ocean, the shelf has been

reported to account for up to 80% of the Ra budget (Kipp et al., 2018). The radium margin flux term accounts for diffusion from shelf sediment via decay of the parent Th isotopes in those sediments; it may also include submarine groundwater discharge or cold seeps as additional Ra sources to the margins. Although Ba fluxes from the margin are not contingent on radioactive decay, Ba also diffuses from the sediment and, thus, Ra and Ba are often linearly correlated in seawater (the sources of Ba to the margins are discussed further in section 5.4). We take advantage of this relationship to independently calculate F_{margin} by utilizing the dissolved barium to radium (dBa:dRa) ratio over the Chukchi shelf (Supplementary Text S5) and the Ra margin flux ($F_{Ra.margin}$, Eqn 10). This analysis determines F_{margin} of Ba, under the assumption that the sources of both elements are similar; we note this is only an approximation since there are some differences in the sources for these two elements.

$$F_{margin} \simeq \frac{dBa}{dRa} \times F_{Ra.margin} \qquad \text{(Eqn. 10)}$$

Following equation 10, we estimated a margin flux of Ba accounting for 41% (range: 23 – 97%) of the inputs relative to sinks, which effectively closes the mass balance. To summarize, our flux balance approach indicates ~50% of the Ba budget must come from an additional source (i.e., F_{margin} F_{ice}, or $-F_{particles}$), which we hypothesized was likely the continental margins. Similarly, the Ba:Ra ratio, suggested ~40% of the Ba budget is derived from the margins, thereby supporting our hypothesis.

We estimated that the net non-conservative component of the budget was 51% (range: 45 - 56%) during the 1994 Arctic Ocean Survey. Our data, within the uncertainties of the method, thus, do not reflect an increase in the net non-conservative flux of Ba between 1994 and 2015. We expected an increase in the margin Ba flux term following findings that radium flux has increased between 2007 and 2015 (Kipp et al., 2018). Indeed, as Arctic Ocean shelves become more frequently ice-free, shelf chemical fluxes to the Arctic Ocean will increase (Charette et al., 2020; Kipp et al., 2018). We acknowledge that our stated uncertainties suggest that our model may not be sensitive enough to detect Ba changes. However, this may also indicate different sources of Ba and Ra to shelf waters. We cannot say for certain; however, between 1994 and 2015, the Ba mass balance was most sensitive to changes in volume fluxes. In contrast, the Ra budget appears to be more sensitive to the change in concentration. Thus, it is possible that the

Ba model is not sensitive enough to capture any change in margin fluxes due to only minor changes in concentration.

5.4 Supply of shelf-derived Ba to the Arctic Ocean basins

Above, we have argued that the Arctic Ocean margins are a significant source of dBa, accounting for roughly half of the Ba budget in the upper 500 m of the Arctic Ocean. By investigating the distributions of dBa in the CAA and the North American, central, and Eurasian Arctic Ocean it appears the largest dBa sources are from North American Arctic Ocean margins (see Section 4.1). This contrast may relate to the shallowness of the North American shelves as compared to the deeper Barents Sea and the regions of the CAA or to the relative nutrient supply and intensity of the local biological pump. To rule out conservative mixing of riverine sources, seawater sources, and sea ice sources we assembled an isotope model and a box model. This box model identified a substantial (~ 50 % of the budget) non-conservative source which we attributed to sedimentary flux of Ba from the margins. To determine if such a dBa flux is reasonable we divided the annual flux (~1 x 10^{10} mol yr^{-1}) by the area of shallow shelves in the Arctic (5.1 × 10^{12} m^2) and determined a shelf normalized dBa flux of 6 µmol m^{-2} d^{-1}. Although the mass balance assumes a well-mixed and evenly distributed source to the upper 500 m of the water column, the distribution of high dBa in the basins indicates a more North American Arctic Ocean source than Eurasian Arctic Ocean and higher concentrations over shallow North American Arctic shelves than the deeper Barents Sea in the Eurasian Arctic. To consider variation of fluxes by different shelf regions, we also estimated the flux with modified shelf area estimates. Using only the area of shallow broad shelves (~ 2.9 × 10^{12} m^2) including the Chukchi, East Siberian, Laptev, and Kara shelves; Jakobsson, 2002) dBa flux was 10 µmol m^{-2} d^{-1}; alternatively, using the total shelf area excluding the Barents Sea (~3.5 × 10^{12} m^2) dBa flux was 9 µmol m^{-2} d^{-1}. These results indicate a margin sedimentary flux of up to 10 µmol m^{-2} d^{-1} which matches fluxes determined in other continental margin settings (Table 3).

Table 3. Estimated area fluxes of dBa from Arctic Ocean shelves compared with studies from other regions.

Region		Area Weighted Flux (μmol m^{-2} d^{-1})	Method	Publication
Arctic Ocean	All shelf area	6	Box Model	*This Study*
	All shelves except the Barents Sea	9		
	Chukchi, East Siberian, Laptev, Kara Sea shelves	10		
California Continental Margin	-	< 2	Benthic Chamber	McManus et al., 1998
Tillamook Bay Estuary	-	2	Box Model	Colbert & McManus, 2005
Mississippi Bight	-	35	Box Model	Ho et al., 2019

Here we review possible mechanisms supplying elevated dBa on the margins: (1) authigenic particulate Ba formation and dissolution and (2) continental sources of Ba.

First we consider marine, authigenic, particle formation as a mechanism to redistribute dBa from shelf surface waters to shelf bottom waters. Authigenic pBa formation on the shelf may be associated with biological activity (e.g., Colbert & McManus, 2005; Hendry et al., 2018; McManus et al., 1994; Thomas et al., 2011), particle scavenging (Dymond et al., 1992), and brine-driven particulate barite formation (Hoppema et al., 2010). Considering observations from the Arctic Ocean's Laptev Sea, Roeske et al. (2012a) hypothesized that vertical redistribution of dBa on the shelves, through particle formation at the surface and dissolution in the bottom waters, and subsequent advection to the basins supported the basin $Ba_{anomaly}$ profiles. Arctic Ocean margin sediments often have high biogenic barium content, especially in association with the ice edge (Nurnberg, 1996). However, for vertical redistribution to support our dBa and $\delta^{138}Ba$ distribution in the basin, a substantial spatial or temporal (e.g., > 10 years) decoupling between surface and bottom shelf waters would be required. Specifically, our mass balance is integrated

over the upper 500 m of the water column, which includes laterally advected surface and bottom shelf waters. Therefore, in conjunction with the $Ba_{anomaly}$ discussion (Section 5.1) dBa cannot simply be moved from the surface to the bottom shelf waters and a sedimentary component must be considered.

Our isotope distribution would require the same temporal decoupling to explain lighter isotopes than predicted in the PH. Indeed, sedimentary Ba does appear to be isotopically light, with excess or authigenic Ba having a δ^{138}Ba of ~0.1 and detrital Ba being even lighter (δ^{138}Ba ~ -0.1 to 0.0) (Bridgestock et al., 2018). It seems unlikely that sedimentary marine pBa is the source of the isotopically light Ba our mass balance demands: the formation of the pBa would leave the water isotopically heavy and the formation and dissolution of excess Ba would need to be spatially or temporally (> 10 years) segregated to provide a net isotopically light Ba signal to the upper water column of the Arctic Ocean (Figure 6). We conclude that authigenic pBa formation alone cannot account for the shelf source.

Continental sources often have high dBa and low δ^{138}Ba (Gaillardet et al., 2014; Gou et al., 2020; Mayfield et al., 2021). Delivery of continental dBa to the marine system could be through river discharge, submarine groundwater discharge, and terrigenous particles. Through our previous sections (Section 5.1 and 5.3) we have demonstrated rivers alone cannot support high dBa concentrations. Submarine groundwater discharge (SGD) has high dBa fluxes and light δ^{138}Ba (e.g., Mayfield et al., 2021; Shaw et al., 1998); however, few studies have examined SGD fluxes in the Arctic shelf system. Although the overall impact and biogeochemical implications (especially for Ba) are presently unknown, site studies in the coastal region of northern Alaska and in the Laptev Sea describe highly variable SGD fluxes (Charkin et al., 2017; Lecher, 2017; Lecher et al., 2016). It is also likely that, as permafrost thaws, SGD fluxes will increase (Lecher, 2017 and references therein) and, thus, the SGD component may become even more important to quantify. Through our investigation we cannot rule out continental sources of Ba to shelf sediments as a source. It is thus possible that terrigenous sources, such as SGD or terrigenous particles, could produce the observed increase in dBa and decrease in the dBa isotopic composition in North American Arctic Ocean halocline waters.

Considering a margin source of dBa is an important exercise in light of recent climate change impacts in the Arctic. Studies suggest that as ice melt recedes, shelf-based sedimentary fluxes to the water column may increase as a result of elevated wind-driven turbulence (e.g.,

Kipp et al., 2018; Charette et al., 2020). Furthermore, changes to productivity due to elongated growing seasons and to particle cycling on the shelves may impact the Ba cycle through biogenic Ba formation and scavenging. The convective mixing regimes over the continental shelves will also change as sea ice retreats. Initially, this may result in greater convective mixing over the shelves in winter months due to an increase in total sea ice formation over the shelves. Kipp et al. (2020b) hypothesized increased mixing on the North American Arctic shelves during winter could allow for larger inputs of benthic materials than observed in summer. Thus, there may be an important seasonal cycle to address in the observed dBa distributions. Different Arctic Ocean shelf regions are likely to have unique responses to changing climatological regimes: the depth of the shelves (and amount of local resuspension), the relative nutrient supply, and the severity of the biological pump must be considered. Furthermore, the nature and quantification of the benthic contribution to the margin flux also needs to be further constrained. This, too, could be a factor contributing to our observation of different relative shelf fluxes between the North American and Eurasian Arctic Oceans and may be climate responsive: to what degree are the margin Ba sources of authigenic or terrigenous origin in different margin settings?

5.5 Arctic Ocean Deep Water Ba

North American Arctic Ocean deep waters had higher dBa (up to 53 nmol kg^{-1}) than Eurasian Arctic Ocean deep waters (up to 47 nmol kg^{-1}). Baffin Bay deep waters had the highest deep dBa concentrations (> 90 nmol kg^{-1}). Several features could explain deep basin dBa distributions including differences in particle supply, origin of particle supply, relative shelf brine contributions, and age of the deep waters. In this section, we assess the likelihood of hydrothermal Ba sources, diffusion from benthic sediments, and particle supply (and dissolution) as potential drivers of deep basin dBa distributions in the North American Arctic Ocean, the Eurasian Arctic Ocean, and Baffin Bay.

Hydrothermal sources are present in the Eurasian Arctic Ocean along the Nansen-Gakkel Ridge, an ultra-slow spreading center (Edmonds et al., 2003); this spreading center has been a source of trace elements in waters deeper than 1000 m (Edmonds et al., 2003; Klunder et al., 2012), but there are no studies investigating the supply of Ba from the Nansen-Gakkel Ridge system. Dissolved Ba in hydrothermal fluids is often high and when high Ba hydrothermal fluids

interact with sulfate rich seawater Barite precipitates, which substantially decreases the effective dBa flux from hydrothermal systems (Eickmann et al., 2014; Hanor, 2000; Jamieson et al., 2016). In this study, a peak of Ba between 2000 and 3000 m is evident at the station nearest the Nansen-Gakkel ridge crest (Supplementary Figure S6); this feature matches, by depth range, dFe and dMn peaks observed in previous studies (Edmonds et al., 2003; Klunder et al., 2012; Middag et al., 2011). Although we identify that dBa flux is occurring from the ridge crest, we cannot quantify the hydrothermal flux and the range of influence in the deep basin in the scope of this study. Recent work indicated the composition of hydrothermal δ^{138}Ba is heavy (Hsieh et al., 2021). To date, there have been no δ^{138}Ba measurements made in the deep Eurasian Basin and efforts to analyze δ^{138}Ba measurements in the Arctic will be important for deconvolving the origin and supply of deep basin Ba.

Diffusion from sediment pore waters is another potential source of dBa. Unfortunately, this synthesis cannot directly assess the scope of this source to the water column in each basin. However, recent work suggests a diffusive benthic source of tracers to Baffin Bay Deep waters (Manning et al., 2020); this idea is supported by the vertical gradient in dBa (i.e., increasing toward the sediments). Importantly, diffusion from sediment pore waters is likely not distinct from dissolution of particles.

Dissolution of particles may also increase deep basin dBa. Deep waters in all Arctic Ocean basins were undersaturated with respect to barite (Figure 2) and thus, particle dissolution could drive increases in dBa. Barium particles to the deep basins may be from local surface production and vertical settling, advected shelf particles (by local currents or eddies) and subsequent vertical settling, injection pumps (such as sinking of brines), subduction of waters, or nepheloid layers.

Nepheloid layers and eddies have been identified as potential sources of particles to the North American Arctic Ocean deep waters (Hunkins et al., 1969; Hwang et al., 2015; Xiang & Lam, 2020) and nepheloid layers were suggested as an explanation of apparent scavenging of dissolved iron in the deep Baffin Bay (Colombo et al., 2020). Additionally, Roeske et al. (2012b) indicated that North American Arctic Ocean deep waters are characterized by dissolution of shelf-derived particles; which may be from the delivery of shelf-derived brines (e.g., Bauch et al., 1995) or from gravitational settling (Boyd et al., 2019; Roeske et al., 2012a).

We consider the feasibility of particle dissolution as a source to the deep dBa by investigating the δ^{138}Ba decrease below 2000 m in the North American Arctic Ocean (Figure 6). Here we calculate the δ^{138}Ba from an additional source (such as dissolving particles) required to decrease the isotopic signature using a simple two component mixing model such that:

$$\delta^{138}Ba_{source} = \frac{(\delta^{138}Ba_{obs} \times dBa_{obs}) - (\delta^{138}Ba_{initial} \times dBa_{initial})}{dBa_{obs} - dBa_{initial}} \quad \text{(Eqn. 11)}$$

The $\delta^{138}Ba_{source}$ was determined to be ~ 0.06 ‰ if deep North American Arctic Ocean waters ($\delta^{138}Ba_{obs}$ = 0.46 ± 0.01 ‰; dBa_{obs} = 52.5 nmol kg^{-1}) were strictly Atlantic in origin ($dBa_{initial}$ = 42 nmol kg^{-1} and $\delta^{138}Ba_{initial}$ = 0.55 ‰). In this scenario, the observed composition is the result of mixing the initial Atlantic-derived seawater with a single source (which realistically may be the net composition of multiple sources). This calculation assumes no mechanism for the additional source (or net isotopes of several sources); yet, we compared the value of $\delta^{138}Ba_{source}$ to references of particle δ^{138}Ba in the literature and note that our estimate agrees with the composition of nonlithogenic particles in sediments in the North Pacific (-0.09 ‰ > $\delta^{138}Ba_{nonlithogenic}$ < 0.10 ‰; Bridgestock et al., 2018; Nielsen et al., 2020).

We further assess the initial conditions in which those particles would have formed by assuming δ^{138}Ba fractionation is between -0.3 and -0.5 (von Allmen et al., 2010; Bridgestock et al., 2018); fractionation. Fractionation of δ^{138}Ba occurs as particles form, but not when they dissolve. The δ^{138}Ba of the source waters can, therefore, be estimated from $\delta^{138}Ba_{source}$ by correcting for the fractionation factor. We estimate the isotopic composition of the dissolved waters the particles formed from range between 0.36 ‰ and 0.56 ‰. The upper 300 m of the basin water column tends to have a dissolved δ^{138}Ba signature near 0.35 ‰ (Figure 6) and the shelf ranges between 0.35 ‰ (near the sediments) and 0.65 (near the surface) (Figure 7).

In the North American Arctic Ocean, isotopic analysis supports water column dissolution of vertically settling or injected upper water column particles as a principal source of the North American Arctic Ocean deep basin dBa signature, however, it does not exclude other sources. Benthic sources are a possibility (and not necessarily distinct from sinking particles). In the Eurasian Arctic Ocean, particle supply through vertical settling is generally low relative to other oceanic regions and when compared to the North American Arctic Ocean (Hwang et al., 2015; Nöthig et al., 2020); although, here too, some particles may be delivered to the deep Eurasian

basin through brine injection and subduction (Dorothea Bauch et al., 1995; Boyd et al., 2019). In this region, the combination of particle dissolution and hydrothermal supply likely influences deep basin dBa distributions; isotopic analyses will be important to quantify the scope of each of these sources. Lastly in Baffin Bay, elevated dBa and pBa signals may be indicative of a nepheloid layer (Figure 3). Furthermore, an active seasonal biological pump could be important in Baffin Bay (Honjo et al., 2010; Lalande et al., 2009; Lehmann et al., 2019; Nöthig et al., 2020). Lemaitre et al.'s (2018) observation high pBa in the deep Labrador Sea which was thought to be the result of bloom cycles and convective downwelling; a similar mechanism may be at play in northern Baffin Bay as well.

5.6 Ba in the Canadian Arctic Archipelago

Transit through the Canadian Arctic Archipelago (CAA) is one of two main pathways for water to exit the Arctic Ocean (Rudels, 2018). Our discussion above suggests the potential for the CAA transit to influence the outgoing Ba distribution, particularly by introduction of river waters and sediment-water column exchange. To consider this influence on dBa, we focus on the Parry Channel Section, which is the channel running between McLure Strait (Figure 8a, #3) and Lancaster Sound (Figure 8a, #6). This channel is a conduit for North American Arctic Ocean waters leaving the Arctic domain through Baffin Bay (e.g., Colombo et al., 2019). Generally, the distributions we observed in the Parry Channel and Lancaster Sound agree with previous observations described in Thomas et al. (2011).

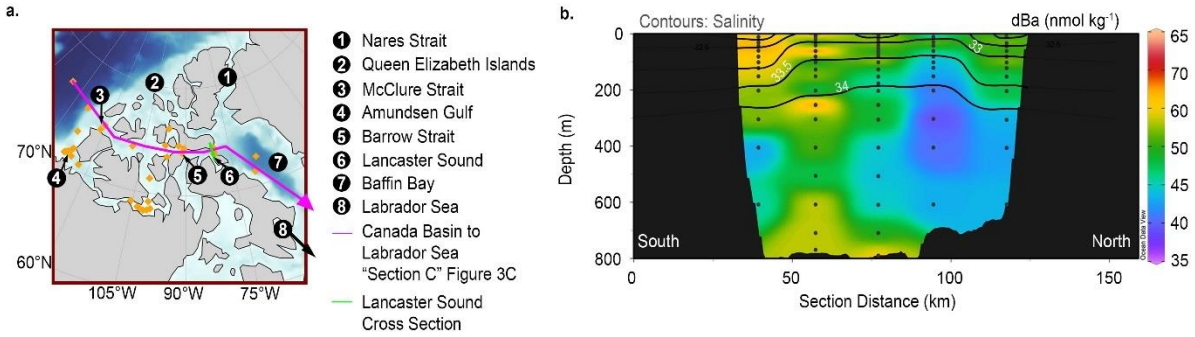

Figure 8. Dissolved Ba distributions in the Canadian Arctic Archipelago. a) geography of the CAA with pertinent features numbered and labeled. Sections investigated in this study are

identified by purple and green lines. b) a cross section of the Lancaster sound depicting dBa on the z-axis; this cross section includes salinity contours from 32 – 34.5 at intervals of 0.5.

In the Parry Channel, the dBa distribution shows the influence of the PH west of Barrow Strait (Figure 3c.1). These waters are typified by high dBa concentrations (~65 nmol kg^{-1}) at densities associated with the PH. Near the Barrow Strait, isopycnals associated with the PH (σ_θ ~ 27.5 kg m^{-3}) shoal and dBa decreases by roughly 10 nmol kg^{-1}. This decrease could be driven by a few mechanisms: (1) sea ice melt, (2) dilution by local rivers, (3) particle formation in surface waters or (4) dilution with low Ba seawater. Although rivers in the CAA have dBa between ~10 – 300 nmol L^{-1} (Colombo et al., 2019b), the decrease in dBa across Barrow Strait occurs at salinities between 32 and 33, and is not correlated to decreasing salinity, which excludes sea ice melt or river discharge as drivers of the dBa decrease (Supplementary Figure S7).

We suspect the dBa decrease eastward in the CAA is driven, in part, by mixing with "Baffin Bay-derived" waters. Specifically, in the Lancaster Sound cross section (Figure 8b) the Ba distribution reveals the influence of at least two water types: high dBa (~55 nmol kg^{-1}; S < 33.5) and low dBa (~45 nmol kg^{-1}; S > 33.5) (Figure 8b). Surface dBa at all Lancaster Sound stations is roughly 55 nmol kg^{-1}. Below the surface layer, the dBa on the northern side of the Sound decreases to ~45 nmol kg^{-1}, while the stations on the south side tend to remain around 55 nmol kg^{-1}. These observations are consistent with the local circulation wherein Baffin Bay-derived waters flow westward on the northern side of the Sound and CAA-derived waters flow eastward on the southern side of the Sound (Prinsenberg et al., 2009). Thus, Baffin Bay-derived waters have the potential to erode the PH signal near Barrow Strait since they contain lower dBa. Thomas et al. (2011) and Mears et al. (2020) described the same dilution effect in the eastern CAA and also attributed it to Atlantic-origin waters in Baffin Bay entering Parry Channel. Furthermore, the same effect has been described for other tracers (e.g., Colombo et al., 2019a; Mears et al., 2020; Rudels, 1986; Top et al., 1980).

Particulate Ba patterns imply that a combination of surface productivity (generating nonlithogenic barite), water mass mixing (driving pBa low in the subsurface), and sediment resuspension (as a source of lithogenic pBa in bottom waters) set the distribution. However, with low pBa concentrations observed, it is likely that the scale of the pBa cycle does not substantially

influence the dBa distribution on relevant timescales in this section. Thus, mixing of water masses remains the likely driver of the dBa distribution.

Flux of dBa across Lancaster Sound, as the product of the Lancaster Sound cross-sectional mean (± 1 SD) and the range of net volume fluxes through Lancaster Sound into Baffin Bay (0.7 ± 0.3 Sv from Prinsenberg et al., 2009) is $1.1 \pm 0.6 \times 10^9$ mol y^{-1}. This is slightly less than, though on the same order of magnitude as other estimates of dBa outflow through Lancaster Sound (Thomas et al., 2011; 1.6×10^9 mol y^{-1}) and through the CAA (Taylor et al., 2003; $2.8 \pm 0.2 \times 10^9$ mol y^{-1}).

The section through Baffin Bay (Figure 3c.1) depicts high (~ 55 nmol kg^{-1}) dBa in surface waters to Davis Strait. Below ~100 m (σ_θ ~ 27 kg m^{-3}) concentrations decline to 40 - 45 nmol kg^{-1}. In Baffin Bay, dBa increases again below the depth of the CAA and Davis Strait sills (~1000 m), yielding dBa concentrations that are higher than observed in any other Arctic region, reaching ~105 nmol kg^{-1} (see section 5.5 for further discussion). South of Baffin Bay, in the Labrador Sea, surface dBa concentrations are low (much more "Atlantic-like", ~ 42 nmol kg^{-1}) and influence from Baffin Bay high dBa values is not evident (Figure 2c). This suggests that there is drawdown of the surface dBa by dilution or internal cycling or that the locations sampled did not capture the outflow of Davis Strait.

Compared to our observations on the Bering and Chukchi Seas, and in the PH of the North American Arctic Ocean, the CAA shows minimal evidence of riverine influence or sedimentary sources on the dBa distribution. This result is unexpected; while one could invoke short residence times of water mass transit (~ 2 years in the CAA for near surface waters, increasing residence time with deeper water masses; Rudels, 1986) the transit across the CAA is longer than that of waters of the Chukchi Shelf (6-8 months; Spall, 2007) and comparable to that of the East Siberian Arctic Seas (~ 6 months to 3.5 years; Bauch et al., 2009; Schlosser et al., 1995). Thus, we're inclined to suggest that the time waters spend on the shelf does not dictate the amount of shelf influence to the region. Geography and geology in the CAA is highly variable (e.g., Colombo et al., 2019a). The CAA stations we investigated in this study have bottom depths > 130 m (sill depth of Barrow Strait; Melling, 2000). Water column depth may be an important dictator of sediment-water column exchange as wind-driven turbulence may support higher levels of sedimentary exchange.

6 Conclusions

We conclude, through observations from 4 synoptic GEOTRACES expeditions, that Ba is not conservative in the Arctic Ocean. Previous studies have noted that non-conservative behavior of dBa in the Arctic Ocean complicates its use as a tracer of river water sources (Hendry et al., 2018; Roeske et al., 2012a). Our pan-Arctic analysis, including dissolved and particulate data as well as isotopic composition, indicates that there is a substantial (~50%) Ba source term from the margin that cannot be accounted for solely by redistribution of dBa in the surface 500 m of the water column. We suggest the application of dBa as a tracer only when the user can verify that inputs from the margins are small and that formation of pBa is not a substantial removal term.

Over the long residence times of deepwater in the basins, particle supply and dissolution may be a dBa source. In the North American Arctic Ocean, the composition of barium isotopes in deep water are lighter than Atlantic derived seawater. The lighter isotopic signature is compatible with dissolution of particles formed in surface waters over the Chukchi Shelf. This conclusion is consistent with previous literature (Roeske et al., 2012b) which used ratios of Ba:Si and Ba:Al to determine there was likely a substantial component of shelf material supplying the deep basin geochemical signatures. Through this study we cannot constrain the deep basin source of Ba strictly to particulate supply and dissolution; yet, the available observations support that hypothesis.

The large margin Ba source reinforces the importance of contributions from the margins to basin geochemical distributions in the Arctic Ocean specifically (Charette et al., 2020; Jensen et al., 2019; Kadko et al., 2019; Kipp et al., 2018; Kondo et al., 2016; Marsay et al., 2018; Whitmore et al., 2019; Xiang & Lam, 2020), and perhaps more generally to the open oceans. Furthermore, it affirms the need to identify and quantify margin inputs at regional scales (e.g., Charette et al., 2016; Jeandel et al., 2011). This is evident from the large non-conservative North American Arctic Ocean dBa signal in the surface 500 m relative to Eurasian Arctic Ocean. Additionally, the CAA dBa distribution is controlled by physical mixing of sea waters and we saw no evidence for a large benthic signal.

We suggest that further investigation into the sedimentary and particulate components of the Ba cycle is necessary. Comprehensive determination of barium concentrations, isotopes, and

fluxes from sediments as well as settling particle fluxes and composition will improve our understanding of the Arctic Ocean barium cycle and allow us to better constrain the geochemical mass balance. Both measurements of *in situ* barium concentrations and isotope composition as well as the composition of potential source materials (e.g., terrigenous particles, marine particles, submarine groundwater discharge, fluvial and estuarine waters) are imperative to these efforts. Such constraints may allow us to better predict the way changing climate will impact dBa distributions and their applications in the Arctic Ocean. Furthermore, we acknowledge there is still great uncertainty into how Arctic Ocean deep basins get and maintain their geochemical signatures. In both the upper water column and deep basins, combined tracer approaches are an important direction to resolving the relative sources and sinks to each basin.

Acknowledgments

This research was supported by the National Science Foundation [OCE-1434312 (AMS), OCE-1436666 (RN), OCE-1535884 (PL), OCE-1736949 and OCE-2023456 (TJH)], Natural Sciences and Engineering Research Council of Canada (NSERC)-Climate Change and Atmospheric Research (CCAR) Program (MTM), and LEFE-CYBER EXPATE (HP). HT acknowledges support by the Canadian GEOTRACES via NSERC-CCAR and the German Academic Exchange Service (DAAD): MOPGA-GRI (Make Our Planet Great Again – Research Initiative) sponsored by BMBF (Federal German Ministry of Education and Research; Grant No. 57429828).

We thank the laboratory technicians that helped produce the data presented in this study: Melissa Gilbert (USM), Jacques Navez (VUB), Martine Leermakers (VUB), and Mette Kaufman (UAF). Christopher Guay contributed dissolved barium data from the 1994 Arctic Ocean Survey. Thank you to the scientific and operational crews of the USCGC Healy (GN01), the CCGS Amundsen (GN02 & GN03), and the R/V Polarstern (GN04). We have great appreciation for the support of the scientific PIs of the four cruises: Greg Cutter (GN01), Roger Francois (GN02 & GN03), Dave Kadko (GN01), Bill Landing (GN01), Kristin Orians (GN03), Michiel Rutgers van der Loeff (GN04), Ursula Schauer (GN04), and Phillipe Tortell (GN02).

Data

Data used in this study are available at the Biological and Chemical Oceanography Data Management Office (DOIs: 10.26008/1912/bco-dmo.772645.2, 10.26008/1912/bco-dmo.807340.1), the EarthChem Library (DOI: 10.1594/IEDA/100633), and PANGAEA (DOI: https://doi.org/10.1594/PANGAEA.896022).

References

Abrahamsen, E. P., Meredith, M. P., Falkner, K. K., Torres-Valdes, S., Leng, M. J., Alkire, M. B., et al. (2009). Tracer-derived freshwater composition of the Siberian continental shelf and slope following the extreme Arctic summer of 2007: Siberian freshwater. *Geophysical Research Letters*, *36*(7), L07602. https://doi.org/10.1029/2009GL037341

Aguilar-Islas, A. M., Rember, R., Nishino, S., Kikuchi, T., & Itoh, M. (2013). Partitioning and lateral transport of iron to the Canada Basin. *Polar Science*, *7*(2), 82–99. https://doi.org/10.1016/j.polar.2012.11.001

Alkire, M. B., Morison, J., & Andersen, R. (2015). Variability in the meteoric water, sea-ice melt, and Pacific water contributions to the central Arctic Ocean, 2000-2014. *Journal of Geophysical Research: Oceans*, *120*(3), 1573–1598. https://doi.org/10.1002/2014JC010023

Alkire, M. B., Jacobson, A. D., Lehn, G. O., Macdonald, R. W., & Rossi, M. W. (2017). On the geochemical heterogeneity of rivers draining into the straits and channels of the Canadian Arctic Archipelago: Canadian Arctic rivers. *Journal of Geophysical Research: Biogeosciences*, *122*(10), 2527–2547. https://doi.org/10.1002/2016JG003723

von Allmen, K., Böttcher, M. E., Samankassou, E., & Nägler, T. F. (2010). Barium isotope fractionation in the global barium cycle: First evidence from barium minerals and precipitation experiments. *Chemical Geology*, *277*(1–2), 70–77. https://doi.org/10.1016/j.chemgeo.2010.07.011

Andersson, P. S., Porcelli, D., Frank, M., Björk, G., Dahlqvist, R., & Gustafsson, Ö. (2008). Neodymium isotopes in seawater from the Barents Sea and Fram Strait Arctic–Atlantic gateways. *Geochimica et Cosmochimica Acta*, *72*(12), 2854–2867. https://doi.org/10.1016/j.gca.2008.04.008

Bates, S. L., Hendry, K. R., Pryer, H. V., Kinsley, C. W., Pyle, K. M., Woodward, E. M. S., & Horner, T. J. (2017). Barium isotopes reveal role of ocean circulation on barium cycling in the Atlantic. *Geochimica et Cosmochimica Acta*, *204*, 286–299. https://doi.org/10.1016/j.gca.2017.01.043

Bauch, D., Dmitrenko, I., Kirillov, S., Wegner, C., Hölemann, J., Pivovarov, S., et al. (2009). Eurasian Arctic shelf hydrography: Exchange and residence time of southern Laptev Sea waters. *Continental Shelf Research*, *29*(15), 1815–1820. https://doi.org/10.1016/j.csr.2009.06.009

Bauch, Dorothea, Schlosser, P., & Fairbanks, R. (1995). Freshwater balance and the sources of deep and bottom waters in the Arctic Ocean inferred from the distribution of $H_2{}^{18}O$. *Progress in Oceanography*, *35*, 53–80.

Beszczynska-Möller, A., Woodgate, R., Lee, C., Melling, H., & Karcher, M. (2011). A Synthesis of Exchanges Through the Main Oceanic Gateways to the Arctic Ocean. *Oceanography*, *24*(3), 82–99. https://doi.org/10.5670/oceanog.2011.59

Beszczynska-Möller, A., Fahrbach, E., Schauer, U., & Hansen, E. (2012). Variability in Atlantic water temperature and transport at the entrance to the Arctic Ocean, 1997–2010. *ICES Journal of Marine Science*, *69*(5), 852–863. https://doi.org/10.1093/icesjms/fss056

Bishop, J. K. B. (1988). The barite-opal-organic carbon association in oceanic particulate matter. *Nature*, *332*.

Boyd, P. W., Claustre, H., Levy, M., Siegel, D. A., & Weber, T. (2019). Multi-faceted particle pumps drive carbon sequestration in the ocean. *Nature*, *568*, 9. https://doi.org/10.1038/s41586-019-1098-2

Bridgestock, L., Hsieh, Y.-T., Porcelli, D., Homoky, W. B., Bryan, A., & Henderson, G. M. (2018). Controls on the barium isotope compositions of marine sediments. *Earth and Planetary Science Letters*, *481*, 101–110. https://doi.org/10.1016/j.epsl.2017.10.019

Cao, Z., Siebert, C., Hathorne, E. C., Dai, M., & Frank, M. (2020). Corrigendum to "Constraining the oceanic barium cycle with stable barium isotopes" [Earth Planet. Sci. Lett. 434 (2016) 1–9]. *Earth and Planetary Science Letters*, *530*, 116003. https://doi.org/10.1016/j.epsl.2019.116003

Cardinal, D., Savoye, N., Trull, T. W., André, L., Kopczynska, E. E., & Dehairs, F. (2005). Variations of carbon remineralisation in the Southern Ocean illustrated by the Baxs proxy. *Deep Sea Research Part I: Oceanographic Research Papers*, *52*(2), 355–370. https://doi.org/10.1016/j.dsr.2004.10.002

Carmack, E. C., Yamamoto-Kawai, M., Haine, T. W. N., Bacon, S., Bluhm, B. A., Lique, C., et al. (2016). Freshwater and its role in the Arctic Marine System: Sources, disposition, storage, export, and physical and biogeochemical consequences in the Arctic and global oceans: Freswater and the Arctic Marine System. *Journal of Geophysical Research: Biogeosciences*, *121*(3), 675–717. https://doi.org/10.1002/2015JG003140

Carter, S. C., Paytan, A., & Griffith, E. M. (2020). Toward an Improved Understanding of the Marine Barium Cycle and the Application of Marine Barite as a Paleoproductivity Proxy. *Minerals*, *10*(5), 421. https://doi.org/10.3390/min10050421

Chan, L. H., Edmond, J. M., Stallard, R. F., Broecker, W. S., Chung, Y. C., Weiss, R. F., & Ku, T. L. (1976). Radium and barium at GEOSECS station in the Atlantic and Pacific, 10.

Chan, L. H., Drummond, D., Edmond, J. M., & Grant, B. (1977). On the barium data from the Atlantic GEOSECS expedition. *Deep Sea Research*, *24*(7), 613–649. https://doi.org/10.1016/0146-6291(77)90505-7

Charbonnier, Q., Moynier, F., & Bouchez, J. (2018). Barium isotope cosmochemistry and geochemistry. *Science Bulletin*, *63*(6), 385–394. https://doi.org/10.1016/j.scib.2018.01.018

Charette, M. A., Lam, P. J., Lohan, M. C., Kwon, E. Y., Hatje, V., Jeandel, C., et al. (2016). Coastal ocean and shelf-sea biogeochemical cycling of trace elements and isotopes: lessons learned from GEOTRACES. *Philosophical Transactions of the Royal Society A: Mathematical, Physical and Engineering Sciences*, *374*(2081), 20160076. https://doi.org/10.1098/rsta.2016.0076

Charette, M. A., Kipp, L. E., Jensen, L. T., Dabrowski, J. S., & Whitmore, L. M. (2020). The Transpolar Drift as a source of riverine and shelf-derived trace elements to the central Arctic Ocean. *Journal of Geophysical Research: Oceans*.

Charkin, A. N., Rutgers van der Loeff, M., Shakhova, N. E., Gustafsson, Ö., Dudarev, O. V., Cherepnev, M. S., et al. (2017). Discovery and characterization of submarine groundwater discharge in the Siberian Arctic seas: a case study in the Buor-Khaya Gulf, Laptev Sea. *The Cryosphere*, *11*(5), 2305–2327. https://doi.org/10.5194/tc-11-2305-2017

Chow, T. J., & Goldberg, E. D. (1960). On the marine geochemistry of barium. *Geochimica et Cosmochimica Acta*, *20*(3–4), 192–198. https://doi.org/10.1016/0016-7037(60)90073-9

Chung, Y. (1980). Radium-barium-silica correlations and a two-dimensional radium model for the world ocean. *Earth and Planetary Science Letters*, *49*(2), 309–318. https://doi.org/10.1016/0012-821X(80)90074-6

Coachman, L. K., & Barnes, C. A. (1963). The Movement of Atlantic Water in the Arctic Ocean. *Arctic*, *16*(1).

Colbert, D., & McManus, J. (2005). Importance of seasonal variability and coastal processes on estuarine manganese and barium cycling in a Pacific Northwest estuary. *Continental Shelf Research*, *25*(11), 1395–1414. https://doi.org/10.1016/j.csr.2005.02.003

Colombo, M., Brown, K. A., De Vera, J., Bergquist, B. A., & Orians, K. J. (2019). Trace metal geochemistry of remote rivers in the Canadian Arctic Archipelago. *Chemical Geology*, *525*, 479–491. https://doi.org/10.1016/j.chemgeo.2019.08.006

Colombo, M., Rogalla, B., Myers, P. G., Allen, S. E., & Orians, K. J. (2019). Tracing Dissolved Lead Sources in the Canadian Arctic: Insights from the Canadian GEOTRACES Program. *ACS Earth and Space Chemistry*, *3*(7), 1302–1314. https://doi.org/10.1021/acsearthspacechem.9b00083

Colombo, M., Jackson, S. L., Cullen, J. T., & Orians, K. J. (2020). Dissolved iron and manganese in the Canadian Arctic Ocean: On the biogeochemical processes controlling their distributions.

Geochimica et Cosmochimica Acta, *277*, 150–174. https://doi.org/10.1016/j.gca.2020.03.012

Cullen, J. T., & Sherrell, R. M. (1999). Techniques for determination of trace metals in small samples of size-fractionated particulate matter: phytoplankton metals off central California. *Marine Chemistry*, *67*(3–4), 233–247. https://doi.org/10.1016/S0304-4203(99)00060-2

Cutter, G., Andersson, P. S., Codispoti, L. A., Croot, P., Francois, R., Lohan, M., et al. (2014). Sampling and Sample-handling Protocols for GEOTRACES Cruises, *Version 2*. http://www.geotraces.org/library-88/scientific-publications/reports/169-sampling-and-sample-handling-protocols-for-geotraces-cruises

Cutter, G., Kadko, D., & Landing, W. (2019). Bottle data from the CTD-ODF carousel on the GEOTRACES Arctic Section cruise (HLY1502) from August to October 2015 (U.S. GEOTRACES Arctic project). *Biological and Chemical Oceanography Data Management Office (BCO-DMO)., Dataset version 2019-07-29*. https://doi.org/10.1575/1912/bco-dmo.646825.4

De Baar, H. J. W., Timmermans, K. R., Laan, P., De Porto, H. H., Ober, S., Blom, J. J., et al. (2008). Titan: A new facility for ultraclean sampling of trace elements and isotopes in the deep oceans in the international Geotraces program. *Marine Chemistry*, *111*(1–2), 4–21. https://doi.org/10.1016/j.marchem.2007.07.009

Dehairs, F., Chesselet, R., & Jedwab, J. (1980). Discrete suspended particles of barite and the barium cycle in the open ocean. *Earth and Planetary Science Letters*, *49*(2), 528–550. https://doi.org/10.1016/0012-821X(80)90094-1

Dehairs, F., Shopova, D., Ober, S., Veth, C., & Goeyens, L. (1997). Particulate barium stocks and oxygen consumption in the Southern Ocean mesopelagic water column during spring and early summer: relationship with export production. *Deep Sea Research Part II: Topical Studies in Oceanography*, *44*(1–2), 497–516. https://doi.org/10.1016/S0967-0645(96)00072-0

Deng, N., Stack, A. G., Weber, J., Cao, B., De Yoreo, J. J., & Hu, Y. (2019). Organic–mineral interfacial chemistry drives heterogeneous nucleation of Sr-rich $(Ba_x, Sr_{1-x})SO_4$ from undersaturated solution. *Proceedings of the National Academy of Sciences*, *116*(27), 13221–13226. https://doi.org/10.1073/pnas.1821065116

Dickens, G. R., Fewless, T., Thomas, E., & Bralower, T. J. (2003). Excess barite accumulation during the Paleocene-Eocene thermal Maximum: Massive input of dissolved barium from seafloor gas hydrate reservoirs. In S. L. Wing, P. D. Gingerich, B. Schmitz, & E. Thomas, *Causes and consequences of globally warm climates in the early Paleogene*. Geological Society of America. https://doi.org/10.1130/0-8137-2369-8.11

Dymond, J., Suess, E., & Lyle, M. (1992). Barium in deep-sea sediment: a geochemical proxy for paleoproductivity, 19.

Eagle, M., Paytan, A., Arrigo, K. R., van Dijken, G., & Murray, R. W. (2003). A comparison between excess barium and barite as indicators of carbon export. *Paleoceanography*, *18*(1), 1021. https://doi.org/10.1029/2002PA000793

Edmonds, H. N., Michael, P. J., Baker, E. T., Connelly, D. P., Snow, J. E., Langmuir, C. H., et al. (2003). Discovery of abundant hydrothermal venting on the ultraslow-spreading Gakkel ridge in the Arctic Ocean. *Nature*, *421*(6920), 252–256. https://doi.org/10.1038/nature01351

Eickmann, B., Thorseth, I. H., Peters, M., Strauss, H., Bröcker, M., & Pedersen, R. B. (2014). Barite in hydrothermal environments as a recorder of subseafloor processes: a multiple-isotope study from the Loki's Castle vent field. *Geobiology*, *12*(4), 308–321. https://doi.org/10.1111/gbi.12086

Falkner, K. K., Macdonald, R. W., Carmack, E. C., & Weingartner, T. (1994). The Potential of Barium as a Tracer of Arctic Water Masses. In O. M. Johannessen, R. D. Muench, & J. E. Overland (Eds.), *Geophysical Monograph Series* (pp. 63–76). Washington, D. C.: American Geophysical Union. https://doi.org/10.1029/GM085p0063

Fransson, A., Chierici, M., Anderson, L. G., Bussmann, I., Kattner, G., Peter Jones, E., & Swift, J. H. (2001). The importance of shelf processes for the modification of chemical constituents in the waters of the Eurasian Arctic Ocean: Implication for carbon fluxes. *Continental Shelf Research*, *21*(3), 225–242. https://doi.org/10.1016/S0278-4343(00)00088-1

Gaillardet, J., Viers, J., & Dupré, B. (2014). Trace Elements in River Waters. In *Treatise on Geochemistry* (pp. 195–235). Elsevier. https://doi.org/10.1016/B978-0-08-095975-7.00507-6

Ganeshram, R. S., François, R., Commeau, J., & Brown-Leger, S. L. (2003). An experimental investigation of barite formation in seawater. *Geochimica et Cosmochimica Acta*, *67*(14), 2599–2605. https://doi.org/10.1016/S0016-7037(03)00164-9

Geyman, B. M., Ptacek, J. L., LaVigne, M., & Horner, T. J. (2019). Barium in deep-sea bamboo corals: Phase associations, barium stable isotopes, & prospects for paleoceanography. *Earth and Planetary Science Letters*, *525*, 115751. https://doi.org/10.1016/j.epsl.2019.115751

Gong, D., & Pickart, R. S. (2016). Early summer water mass transformation in the eastern Chukchi Sea. *Deep Sea Research Part II: Topical Studies in Oceanography*, *130*, 43–55. https://doi.org/10.1016/j.dsr2.2016.04.015

Gou, L.-F., Jin, Z., Galy, A., Gong, Y.-Z., Nan, X.-Y., Jin, C., et al. (2020). Seasonal riverine barium isotopic variation in the middle Yellow River: Sources and fractionation. *Earth and Planetary Science Letters*, *531*, 115990. https://doi.org/10.1016/j.epsl.2019.115990

Guay, Christopher K., McLaughlin, F. A., & Yamamoto-Kawai, M. (2009). Differentiating fluvial components of upper Canada Basin waters on the basis of measurements of dissolved barium combined with other physical and chemical tracers. *Journal of Geophysical Research*, *114*.

https://doi.org/10.1029/2008JC005099

Guay, C.K., & Falkner, K. K. (1997). Barium as a tracer of Arctic halocline and river waters. *Deep Sea Research Part II: Topical Studies in Oceanography*, *44*(8), 1543–1569. https://doi.org/10.1016/S0967-0645(97)00066-0

Guay, C.K., & Falkner, K. K. (1998). A survey of dissolved barium in the estuaries of major Arctic rivers and adjacent seas. *Continental Shelf Research*, *18*(8), 859–882. https://doi.org/10.1016/S0278-4343(98)00023-5

Haine, T. W. N., Curry, B., Gerdes, R., Hansen, E., Karcher, M., Lee, C., et al. (2015). Arctic freshwater export: Status, mechanisms, and prospects. *Global and Planetary Change*, *125*, 13–35. https://doi.org/10.1016/j.gloplacha.2014.11.013

Hanor, J. S. (2000). Barite–Celestine Geochemistry and Environments of Formation. *Reviews in Mineralogy and Geochemistry*, *40*(1), 193–275. https://doi.org/10.2138/rmg.2000.40.4

Hendry, K. R., Pyle, K. M., Barney Butler, G., Cooper, A., Fransson, A., Chierici, M., et al. (2018). Spatiotemporal Variability of Barium in Arctic Sea-Ice and Seawater. *Journal of Geophysical Research: Oceans*, *123*(5), 3507–3522. https://doi.org/10.1029/2017JC013668

Ho, P., Shim, M. J., Howden, S. D., & Shiller, A. M. (2019). Temporal and spatial distributions of nutrients and trace elements (Ba, Cs, Cr, Fe, Mn, Mo, U, V and Re) in Mississippi coastal waters: Influence of hypoxia, submarine groundwater discharge, and episodic events. *Continental Shelf Research*, *175*, 53–69. https://doi.org/10.1016/j.csr.2019.01.013

Holmes, R. M., McClelland, J. W., Tank, S. E., Spencer, R. G. M., & Shiklomanov, A. I. (2018). Arctic Great Rivers Observatory. Water Quality Dataset, Version 20181010. Retrieved from https://www.arcticgreatrivers.org/data

Honjo, S., Krishfield, R. A., Eglinton, T. I., Manganini, S. J., Kemp, J. N., Doherty, K., et al. (2010). Biological pump processes in the cryopelagic and hemipelagic Arctic Ocean: Canada Basin and Chukchi Rise. *Progress in Oceanography*, *85*(3–4), 137–170. https://doi.org/10.1016/j.pocean.2010.02.009

Hoppema, M., Dehairs, F., Navez, J., Monnin, C., Jeandel, C., Fahrbach, E., & de Baar, H. J. W. (2010). Distribution of barium in the Weddell Gyre: Impact of circulation and biogeochemical processes. *Marine Chemistry*, *122*(1–4), 118–129. https://doi.org/10.1016/j.marchem.2010.07.005

Horner, T., & Crockford, P. (2021). *Barium Isotopes: Drivers, Dependencies, and Distributions through Space and Time*. Cambridge: Cambridge University Press.

Horner, T. J., Kinsley, C. W., & Nielsen, S. G. (2015). Barium-isotopic fractionation in seawater mediated by barite cycling and oceanic circulation. *Earth and Planetary Science Letters*, *430*, 511–522. https://doi.org/10.1016/j.epsl.2015.07.027

Hsieh, Y.-T., & Henderson, G. M. (2017). Barium stable isotopes in the global ocean: Tracer of Ba inputs and utilization. *Earth and Planetary Science Letters*, *473*, 269–278. https://doi.org/10.1016/j.epsl.2017.06.024

Hsieh, Y.-T., Bridgestock, Luke, Scheuermann, Peter P., Seyfried, William E. Jr., & Henderson, Gideon M. (2021). Barium isotopes in mid-ocean ridge hydrothermal vent fluids: A source of isotopically heavy Ba to the ocean. *Geochimica et Cosmochimica Acta*, *292*, 348–363. https://doi.org/10.1016/j.gca.2020.09.037

Hunkins, K., Thorndike, E. M., & Mathieu, G. (1969). Nepheloid layers and bottom currents in the Arctic Ocean. *Journal of Geophysical Research*, *74*(28), 6995–7008. https://doi.org/10.1029/JC074i028p06995

Hwang, J., Kim, M., Manganini, S. J., McIntyre, C. P., Haghipour, N., Park, J., et al. (2015). Temporal and spatial variability of particle transport in the deep Arctic Canada Basin: particle flux in canada basin. *Journal of Geophysical Research: Oceans*, *120*(4), 2784–2799. https://doi.org/10.1002/2014JC010643

Jacquet, S. H. M., Dehairs, F., Cardinal, D., Navez, J., & Delille, B. (2005). Barium distribution across the Southern Ocean frontal system in the Crozet–Kerguelen Basin. *Marine Chemistry*, *95*(3–4), 149–162. https://doi.org/10.1016/j.marchem.2004.09.002

Jakobsson, M. (2002). Hypsometry and volume of the Arctic Ocean and its constituent seas. *Geochemistry, Geophysics, Geosystems*, *3*(5), 1–18. https://doi.org/10.1029/2001GC000302

Jamieson, J. W., Hannington, M. D., Tivey, M. K., Hansteen, T., Williamson, N. M.-B., Stewart, M., et al. (2016). Precipitation and growth of barite within hydrothermal vent deposits from the Endeavour Segment, Juan de Fuca Ridge. *Geochimica et Cosmochimica Acta*, *173*, 64–85. https://doi.org/10.1016/j.gca.2015.10.021

Jeandel, C., Peucker-Ehrenbrink, B., Jones, M. T., Pearce, C. R., Oelkers, E. H., Godderis, Y., et al. (2011). Ocean margins: The missing term in oceanic element budgets? *Eos, Transactions American Geophysical Union*, *92*(26), 217–224. https://doi.org/10.1029/2011EO260001

Jensen, L. T., Wyatt, N. J., Twining, B. S., Rauschenberg, S., Landing, W. M., Sherrell, R. M., & Fitzsimmons, J. N. (2019). Biogeochemical Cycling of Dissolved Zinc in the Western Arctic (Arctic GEOTRACES GN01). *Global Biogeochemical Cycles*, *33*(3), 343–369. https://doi.org/10.1029/2018GB005975

Kadko, D., Aguilar-Islas, A., Bolt, C., Buck, C. S., Fitzsimmons, J. N., Jensen, L. T., et al. (2019). The residence times of trace elements determined in the surface Arctic Ocean during the 2015 US Arctic GEOTRACES expedition. *Marine Chemistry*, *208*, 56–69. https://doi.org/10.1016/j.marchem.2018.10.011

Kipp, L. E., Spall, M. A., Pickart, R. S., Kadko, D. C., Moore, W. S., Dabrowski, J. S., & Charette, M. A. (2020). Observational and Modeling Evidence of Seasonal Trends in Sediment-Derived Material Inputs to the Chukchi Sea. *Journal of Geophysical Research: Oceans*, *125*(5). https://doi.org/10.1029/2019JC016007

Kipp, Lauren E., Charette, M. A., Moore, W. S., Henderson, P. B., & Rigor, I. G. (2018). Increased fluxes of shelf-derived materials to the central Arctic Ocean. *Science Advances*, *4*(1), eaao1302. https://doi.org/10.1126/sciadv.aao1302

Kipp, Lauren E., Kadko, D. C., Pickart, R. S., Henderson, P. B., Moore, W. S., & Charette, M. A. (2019). Shelf-Basin Interactions and Water Mass Residence Times in the Western Arctic Ocean: Insights Provided by Radium Isotopes. *Journal of Geophysical Research: Oceans*, 2019JC014988. https://doi.org/10.1029/2019JC014988

Kipp, Lauren E., Henderson, P. B., Wang, Z. A., & Charette, M. A. (2020). Deltaic and Estuarine Controls on Mackenzie River Solute Fluxes to the Arctic Ocean. *Estuaries and Coasts*. https://doi.org/10.1007/s12237-020-00739-8

Klunder, M. B., Laan, P., Middag, R., de Baar, H. J. W., & Bakker, K. (2012). Dissolved iron in the Arctic Ocean: Important role of hydrothermal sources, shelf input and scavenging removal. *Journal of Geophysical Research: Oceans*, *117*, C04014. https://doi.org/10.1029/2011JC007135

Kondo, Y., Obata, Hajime., Hioki, N., Ooki, A., Nishino, S., Kikuchi, T., & Kuma, K. (2016). Transport of trace metals (Mn, Fe, Ni, Zn and Cd) in the western Arctic Ocean (Chukchi Sea and Canada Basin) in late summer 2012. *Deep Sea Research Part I: Oceanographic Research Papers*, *116*, 236–252. https://doi.org/10.1016/j.dsr.2016.08.010

Lalande, C., Forest, A., Barber, D. G., Gratton, Y., & Fortier, L. (2009). Variability in the annual cycle of vertical particulate organic carbon export on Arctic shelves: Contrasting the Laptev Sea, Northern Baffin Bay and the Beaufort Sea. *Continental Shelf Research*, *29*(17), 2157–2165. https://doi.org/10.1016/j.csr.2009.08.009

Lam, P. (2020). Size-fractionated major and minor particle composition and concentration from the US GEOTRACES Arctic cruise (HLY1502) on USCGC Healy from August to October 2015. (Version (Version 1) Version Date 2020-04-01). Biological and Chemical Oceanographic Data Management Office (BCO-DMO).

Lam, P. J., & Bishop, J. K. B. (2008). The continental margin is a key source of iron to the HNLC North Pacific Ocean. *Geophysical Research Letters*, *35*(7), n/a-n/a. https://doi.org/10.1029/2008GL033294

Lam, P. J., & Marchal, O. (2015). Insights into Particle Cycling from Thorium and Particle Data. *Annual Review of Marine Science*, *7*(1), 159–184. https://doi.org/10.1146/annurev-marine-010814-

015623

Laukert, G., Frank, M., Hathorne, E. C., Krumpen, T., Rabe, B., Bauch, D., et al. (2017). Pathways of Siberian Freshwater and Sea Ice in the Arctic Ocean Traced with Radiogenic Neodymium Isotopes and Rare Earth Elements (Version 1.0) [Application/pdf]. *Polarforschung*, 11 pages. https://doi.org/10.2312/POLARFORSCHUNG.87.1.3

Le Roy, E., Sanial, V., Charette, M. A., van Beek, P., Lacan, F., Jacquet, S. H. M., et al. (2018). The 226Ra–Ba relationship in the North Atlantic during GEOTRACES-GA01. *Biogeosciences*, *15*(9), 3027–3048. https://doi.org/10.5194/bg-15-3027-2018

LeBlond, P. H. (1980). On the Surface Circulation in Some Channels of the Canadian Arctic Archipelago. *ARCTIC*, *33*(1), 189–197. https://doi.org/10.14430/arctic2554

Lecher, A. (2017). Groundwater Discharge in the Arctic: A Review of Studies and Implications for Biogeochemistry. *Hydrology*, *4*(3), 41. https://doi.org/10.3390/hydrology4030041

Lecher, A. L., Kessler, J., Sparrow, K., Garcia-Tigreros Kodovska, F., Dimova, N., Murray, J., et al. (2016). Methane transport through submarine groundwater discharge to the North Pacific and Arctic Ocean at two Alaskan sites: SGD methane transport. *Limnology and Oceanography*, *61*(S1), S344–S355. https://doi.org/10.1002/lno.10118

Lemaitre, N., Planchon, F., Planquette, H., Dehairs, F., Fonseca-Batista, D., Roukaerts, A., et al. (2018). High variability of particulate organic carbon export along the North Atlantic GEOTRACES section GA01 as deduced from ^{234}Th fluxes. *Biogeosciences*, *15*(21), 6417–6437. https://doi.org/10.5194/bg-15-6417-2018

Manning, C., Bourbonnais, A., Granger, J., Hamme, R. C., Yeung, L., Amando Valerio, D., et al. (2020). OB21B-05 - Nitrogen cycling and circulation in Baffin Bay investigated with isotopic measurements of N2, N2O and NO3-. Presented at the Ocean Sciences Meeting, Portland, Oregon: AGU.

Marsay, C. M., Aguilar-Islas, A., Fitzsimmons, J. N., Hatta, M., Jensen, L. T., John, S. G., et al. (2018). Dissolved and particulate trace elements in late summer Arctic melt ponds. *Marine Chemistry*, *204*, 70–85. https://doi.org/10.1016/j.marchem.2018.06.002

Martinez-Ruiz, F., Paytan, A., Gonzalez-Muñoz, M. T., Jroundi, F., Abad, M. M., Lam, P. J., et al. (2019). Barite formation in the ocean: Origin of amorphous and crystalline precipitates. *Chemical Geology*, *511*, 441–451. https://doi.org/10.1016/j.chemgeo.2018.09.011

Mayfield, K. K., Eisenhauer, A., Santiago Ramos, D. P., Higgins, J. A., Horner, T. J., Auro, M., et al. (2021). Groundwater discharge impacts marine isotope budgets of Li, Mg, Ca, Sr, and Ba. *Nature Communications*, *12*(1), 148. https://doi.org/10.1038/s41467-020-20248-3

McClelland, J. W., Holmes, R. M., Dunton, K. H., & Macdonald, R. W. (2012). The Arctic Ocean

Estuary. *Estuaries and Coasts*, *35*(2), 353–368. https://doi.org/10.1007/s12237-010-9357-3

McLaughlin, F. A., Carmack, E. C., Ingram, R. G., Williams, W. J., & Michel, C. (2004). Chapter 31. Oceanography of the Northwest Passage (26,P). In *The Global Coastal Ocean, Interdisciplinary Regional Studies and Syntheses* (pp. 1211–1242). Harvard university Press.

McManus, J., Berelson, W. M., Klinkhammer, G. P., Kilgore, T. E., & Hammond, D. E. (1994). Remobilization of barium in continental margin sediments. *Geochimica et Cosmochimica Acta*, *58*(22), 4899–4907. https://doi.org/10.1016/0016-7037(94)90220-8

McManus, J., Berelson, W. M., Klinkhammer, G. P., Johnson, K. S., Coale, K. H., Anderson, R. F., et al. (1998). Geochemistry of barium in marine sediments: implications for its use as a paleoproxy. *Geochimica et Cosmochimica Acta*, *62*(21–22), 3453–3473. https://doi.org/10.1016/S0016-7037(98)00248-8

Mears, C., Thomas, H., Henderson, P. B., Charette, M. A., MacIntyre, H., Dehairs, F., et al. (2020). Using ^{226}Ra and ^{228}Ra isotopes to distinguish water mass distribution in the Canadian Arctic Archipelago. *Biogeosciences*, *17*(20), 4937–4959. https://doi.org/10.5194/bg-17-4937-2020

Melling, H. (2000). Exchanges of freshwater through the shallow straits of the North American Arctic. In *The Freshwater Budget of the Arctic Ocean* (pp. 479–502). The Netherlands: Kluwer Academic Publishers.

Middag, R., de Baar, H. J. W., Laan, P., & Bakker, K. (2009). Dissolved aluminium and the silicon cycle in the Arctic Ocean. *Marine Chemistry*, *115*(3–4), 176–195. https://doi.org/10.1016/j.marchem.2009.08.002

Middag, R., de Baar, H. J. W., Laan, P., & Klunder, M. B. (2011). Fluvial and hydrothermal input of manganese into the Arctic Ocean. *Geochimica et Cosmochimica Acta*, *75*(9), 2393–2408. https://doi.org/10.1016/j.gca.2011.02.011

Millero, F. J. (1982). The effect of pressure on the solubility of minerals in water and seawater. *Geochimica et Cosmochimica Acta*, *46*(1), 11–22. https://doi.org/10.1016/0016-7037(82)90286-1

Milliman, J. D., & Farnsworth, K. L. (2013). *River Discharge to the Coastal Ocean: a global synthesis*. Cambridge, United Kingdom: Cambridge University Press.

Monnin, C., Jeandel, C., Cattaldo, T., & Dehairs, F. (1999). The marine barite saturation state of the world's oceans. *Marine Chemistry*, *65*(3–4), 253–261. https://doi.org/10.1016/S0304-4203(99)00016-X

N. Lehmann, M. Kienast, J. Granger, A. Bourbonnais, M. A. Altabet, & J.-É. Tremblay. (2019). Remote western Arctic nutrients fuel remineralization in deep Baffin Bay. *Global Biogeochemical Cycles*, *33*, 649–667. https://doi.org/10.1029/2018GB006134

Nancollas, G. H., & Purdie, N. (1963). Crystallization of barium sulphate in aqueous solution.

Transactions of the Faraday Society, *59*, 735. https://doi.org/10.1039/tf9635900735

Newton, R., Schlosser, P., Mortlock, R., Swift, J., & MacDonald, R. (2013). Canadian Basin freshwater sources and changes: Results from the 2005 Arctic Ocean Section: AOS 2005 freshwater sources and changes. *Journal of Geophysical Research: Oceans*, *118*(4), 2133–2154. https://doi.org/10.1002/jgrc.20101

Nielsen, S. G., Shu, Y., Auro, M., Yogodzinski, G., Shinjo, R., Plank, T., et al. (2020). Barium isotope systematics of subduction zones. *Geochimica et Cosmochimica Acta*, *275*, 1–18. https://doi.org/10.1016/j.gca.2020.02.006

Nöthig, E.-M., Lalande, C., Fahl, K., Metfies, K., Salter, I., & Bauerfeind, E. (2020). Annual cycle of downward particle fluxes on each side of the Gakkel Ridge in the central Arctic Ocean. *Philosophical Transactions of the Royal Society A: Mathematical, Physical and Engineering Sciences*, *378*(2181), 20190368. https://doi.org/10.1098/rsta.2019.0368

Ober, S., Rijkenberg, M. J. A., & Gerringa, L. J. A. (2016). Physical oceanography measured with ultra clean CTD/Water sampler-system during POLARSTERN cruise PS94 (ARK-XXIX/3). *Royal Netherlands Institute for Sea Research, Texel*. https://doi.org/10.1594/PANGAEA.859560

Ohnemus, D. C., Auro, M. E., Sherrell, R. M., Lagerström, M., Morton, P. L., Twining, B. S., et al. (2014). Laboratory intercomparison of marine particulate digestions including Piranha: a novel chemical method for dissolution of polyethersulfone filters. *Limnology and Oceanography: Methods*, *12*(8), 530–547. https://doi.org/10.4319/lom.2014.12.530

Peterson, I., Hamilton, J., Prinsenberg, S., & Pettipas, R. (2012). Wind-forcing of volume transport through Lancaster Sound: transport through Lancaster Sound. *Journal of Geophysical Research: Oceans*, *117*(C11018). https://doi.org/10.1029/2012JC008140

Planquette, H., & Sherrell, R. M. (2012). Sampling for particulate trace element determination using water sampling bottles: methodology and comparison to in situ pumps: Particulate trace element sampling. *Limnology and Oceanography: Methods*, *10*(5), 367–388. https://doi.org/10.4319/lom.2012.10.367

Prinsenberg, S., Hamilton, J., Peterson, I., & Pettipas, R. (2009). Observing and interpreting the seasonal variability of the oceanographic fluxes passing through Lancaster Sound of the Canadian Arctic Archipelago. In J. C. J. Nihoul & A. G. Kostianoy (Eds.), *Influence of Climate Change on the Changing Arctic and Sub-Arctic Conditions* (pp. 125–143). Dordrecht: Springer Netherlands. https://doi.org/10.1007/978-1-4020-9460-6_10

R Core Team. (2018). *R: A language and environment for statistical computing.* Vienna, Austria: R foundation for Statistical computing. Retrieved from https://www.R-project.org/

Rember, R. (2018). Dissolved barium measured on water bottle samples during POLARSTERN cruise

PS94 (ARK-XXIX/3) to the central Arctic ocean in 2015. https://doi.org/10.1594/PANGAEA.896022

Roeske, T., Rutgers van der Loeff, M., Middag, R., & Bakker, K. (2012). Deep water circulation and composition in the Arctic Ocean by dissolved barium, aluminium and silicate. *Marine Chemistry*, *132–133*, 56–67. https://doi.org/10.1016/j.marchem.2012.02.001

Roeske, T., Bauch, D., Rutgers van der Loeff, M., & Rabe, B. (2012). Utility of dissolved barium in distinguishing North American from Eurasian runoff in the Arctic Ocean. *Marine Chemistry*, *132–133*, 1–14. https://doi.org/10.1016/j.marchem.2012.01.007

Rudels, B. (1986). The outflow of polar water through the Arctic Archipelago and the oceanographic conditions in Baffin Bay. *Polar Research*, *4*(2), 161–180. https://doi.org/10.3402/polar.v4i2.6929

Rudels, B. (2015). Arctic Ocean circulation, processes and water masses: A description of observations and ideas with focus on the period prior to the International Polar Year 2007–2009. *Progress in Oceanography*, *132*, 22–67. https://doi.org/10.1016/j.pocean.2013.11.006

Rudels, B. (2018). Arctic Ocean Circulation. In *Encyclopedia of Ocean Sciences*. Elsevier. https://doi.org/10.1016/B978-0-12-409548-9.11209-6

Rudels, B., & Quadfasel, D. (1991). Convection and deep water formation in the Arctic Ocean-Greenland Sea System. *Journal of Marine Systems*, *2*(3–4), 435–450. https://doi.org/10.1016/0924-7963(91)90045-V

Rudels, B., Jones, E. P., Schauer, U., & Eriksson, P. (2004). Atlantic sources of the Arctic Ocean surface and halocline waters. *Polar Research*, *23*(2), 181–208. https://doi.org/10.3402/polar.v23i2.6278

Rudnick, R. L., & Gao, S. (2014). 4.1 - Composition of the Continental Crust. In *Treatise on Geochemistry* (2nd ed., pp. 1–51). Oxford: Elsevier.

Rushdi, A. I., McManus, J., & Collier, R. W. (2000). Marine barite and celestite saturation in seawater. *Marine Chemistry*, *69*(1–2), 19–31. https://doi.org/10.1016/S0304-4203(99)00089-4

Schlitzer, R. (2018). Ocean Data View 5.1.5. Retrieved from https://odv.awi.de

Schlitzer, R., Anderson, R. F., & Masferrer Dodas, E. (2018). The GEOTRACES Intermediate Data Product 2017. *Chemical Geology*. https://doi.org/10.1016/J.CHEMGEO.2018.05.040

Schlosser, P., Bayer, R., Bönisch, G., Cooper, L. W., Ekwurzel, B., Jenkins, W. J., et al. (1999). Pathways and mean residence times of dissolved pollutants in the ocean derived from transient tracers and stable isotopes. *Science of The Total Environment*, *237–238*, 15–30. https://doi.org/10.1016/S0048-9697(99)00121-7

Schlosser, Peter, Swift, J. H., Lewis, D., & Pfirman, S. L. (1995). The role of the large-scale Arctic Ocean circulation in the transport of contaminants. *Deep Sea Research Part II: Topical Studies in Oceanography*, *42*(6), 1341–1367. https://doi.org/10.1016/0967-0645(95)00045-3

Shaw, T. J., Moore, W. S., Kloepfer, J., & Sochaski, M. A. (1998). The flux of barium to the coastal waters of the southeastern USA: the importance of submarine groundwater discharge. *Geochimica et Cosmochimica Acta*, *62*(18), 3047–3054. https://doi.org/10.1016/S0016-7037(98)00218-X

Shiller, A. (2019). Dissolved Ba, Cd, Cu, Ga, Mn, Ni, and V concentration data from the US GEOTRACES Arctic Expeditions (GN01, HLY1502) from August to October 2015. *Biological and Chemical Oceanography Data Management Office (BCO-DMO), Dataset version 2019-07-09*. https://doi.org/10.1575/1912/bco-dmo.772645.1

Spall, M. A. (2007). Circulation and water mass transformation in a model of the Chukchi Sea. *Journal of Geophysical Research*, *112*(C5), C05025. https://doi.org/10.1029/2005JC003364

Steele, M., Morison, J., Ermold, W., Rigor, I., Ortmeyer, M., & Shimada, K. (2004). Circulation of summer Pacific halocline water in the Arctic Ocean. *Journal of Geophysical Research*, *109*, C02027. https://doi.org/10.1029/2003JC002009

Talley, L. D., Pickard, G. L., Emery, W. J., & Swift, J. H. (2011). Arctic Ocean and Nordic Seas. In *Descriptive Physical Oceanography* (pp. 401–436). Elsevier. https://doi.org/10.1016/B978-0-7506-4552-2.10012-5

Tanhua, T., Jones, E. P., Jeansson, E., Jutterström, S., Smethie, W. M., Wallace, D. W. R., & Anderson, L. G. (2009). Ventilation of the Arctic Ocean: Mean ages and inventories of anthropogenic CO_2 and CFC-11. *Journal of Geophysical Research*, *114*(C1), C01002. https://doi.org/10.1029/2008JC004868

Taylor, J. R., Falkner, K. K., Schauer, U., & Meredith, M. (2003). Quantitative considerations of dissolved barium as a tracer in the Arctic Ocean. *Journal of Geophysical Research*, *108*(C12), 3374. https://doi.org/10.1029/2002JC001635

Thomas, H., Shadwick, E., Dehairs, F., Lansard, B., Mucci, A., Navez, J., et al. (2011). Barium and carbon fluxes in the Canadian Arctic Archipelago. *Journal of Geophysical Research*, *116*, C00G08. https://doi.org/10.1029/2011JC007120

Timmermans, M.-L., Proshutinsky, A., Golubeva, E., Jackson, J. M., Krishfield, R., McCall, M., et al. (2014). Mechanisms of Pacific Summer Water variability in the Arctic's Central Canada Basin. *Journal of Geophysical Research: Oceans*, *119*(11), 7523–7548. https://doi.org/10.1002/2014JC010273

Top, Z., Clarke, W. B., Eismont, W. C., & Jones, E. P. (1980). Radiogenic helium in Baffin Bay bottom water. *Journal of Marine Research*, 19.

Wassmann, P., Duarte, C. M., Agustí, S., & Sejr, M. K. (2011). Footprints of climate change in the Arctic marine ecosystem. *Global Change Biology*, *17*(2), 1235–1249. https://doi.org/10.1111/j.1365-

2486.2010.02311.x

Weingartner, T. J., Cavalieri, D. J., Aagaard, K., & Sasaki, Y. (1998). Circulation, dense water formation, and outflow on the northeast Chukchi Shelf. *Journal of Geophysical Research: Oceans*, *103*(C4), 7647–7661. https://doi.org/10.1029/98JC00374

Whitmore, L. M., Morton, P. L., Twining, B. S., & Shiller, A. M. (2019). Vanadium cycling in the Western Arctic Ocean is influenced by shelf-basin connectivity. *Marine Chemistry*, *216*, 103701. https://doi.org/10.1016/j.marchem.2019.103701

Whitmore, L. M., Pasqualini, A., Newton, R., & Shiller, A. M. (2020). Gallium: A New Tracer of Pacific Water in the Arctic Ocean. *Journal of Geophysical Research: Oceans*, *125*(7). https://doi.org/10.1029/2019JC015842

Woodgate, R. A., Weingartner, T. J., & Lindsay, R. (2012). Observed increases in Bering Strait oceanic fluxes from the Pacific to the Arctic from 2001 to 2011 and their impacts on the Arctic Ocean water column. *Geophysical Research Letters*, *39*(24), 2012GL054092. https://doi.org/10.1029/2012GL054092

Xiang, Y., & Lam, P. J. (2020). Size-fractionated marine suspended particle dynamics in the Western Arctic Ocean: Lateral and vertical sources. *Journal of Geophysical Research: Oceans*, *125*(8), e2020JC016144.

Yamamoto-Kawai, M., Carmack, E. C., McLaughlin, F. A., & Falkner, K. K. (2010). Oxygen isotope ratio, barium and salinity in waters around the North American coast from the Pacific to the Atlantic: Implications for freshwater sources to the Arctic throughflow. *Journal of Marine Research*, *68*(1), 97–117. https://doi.org/10.1357/002224010793078988

Journal of Geophysical Research: Oceans

Supporting Information for

Strong margin influence on Arctic Ocean barium cycle revealed by Pan-Arctic Synthesis

Laura M. Whitmore[1]*, Alan M. Shiller[1*], Tristan J. Horner[2], Yang Xiang[3], Maureen E. Auro[2], Dorothea Bauch[4], Frank Dehairs[5], Phoebe J. Lam[3], Jingxuan Li[6], Maria T. Maldonado[6], Chantal Mears[7], Robert Newton[8], Angelica Pasqualini[9], Hélène Planquette[10], Robert Rember[11], Helmuth Thomas[7]

[1]School of Ocean Science and Engineering, University of Southern Mississippi, Stennis Space Center, Mississippi, USA; [2]NIRVANA Laboratories, Woods Hole Oceanographic Institution, Woods Hole, MA 02543, USA; [3]Department of Ocean Sciences, University of California, Santa Cruz, CA 95064 USA; [4]GEOMAR Helmholtz Centre for Ocean Research, Kiel, Germany; [5]Analytical, Environmental and Geochemistry, Vrije Universiteit Brussel, 1050 Brussels, Belgium; [6]Earth Ocean & Atmospheric Sciences, University of British Columbia, Vancouver, BC, Canada; [7]Institute for Coastal Research, Helmholtz Centre Geesthacht, Geesthacht, Germany; [8]Lamont-Doherty Earth Observatory, Columbia University; [9]Department of Earth and Environmental Engineering, Columbia University, New York, NY, USA; [10] Univ Brest, CNRS, IRD, Ifremer, LEMAR, F-29280 Plouzane, France; [11]International Arctic Research Center, University of Alaska Fairbanks, Fairbanks, Alaska 99775, USA

Corresponding author: Laura M. Whitmore (lmwhitmore@alaska.edu) and Alan M. Shiller (alan.shiller@usm.edu)

Contents of this file

Introduction

The information in this supplemental includes additional text, tables, and figures. Presented is an expansion on the methods presented in the manuscript, intercalibration of trace element data, and additional supportive figures toward the discussion in the manuscript. Details can be found in the sections below.

Text S1. Additional Sampling and Analytical Protocols for dBa

Filtered seawater was collected into acid-washed 125 mL HDPE bottles. Acid washing procedures met GEOTRACES standards (www.geotraces.org/cookbook): bottles were filled with ~10% HCl (Reagent Grade) and soaked overnight at ~60°C (repeated 3 times). Bottles were then rinsed with DI water. Shipboard sampling was conducted by filtration through a 0.45 micron supor filter, each bottle was rinsed with seawater (3x) before collection of the sample.

GN01

At the University of Southern Mississippi (USM) Center for Trace Analysis, dissolved Ba was determined using an ICP-MS (ThermoFisher Element XR) in low resolution; samples were introduced with a PC3 spray chamber (Elemental Scientific). Prior to analysis, samples were acidified to 0.024 M HCl (Fisher Optima). In preparation for analysis, following isotope dilution methods (Klinkhammer and Chan, 1990), samples were diluted 30-fold with ultra-pure water and spiked with enriched ^{135}Ba solution (Oak Ridge National Laboratory) to a target $^{138/135}$Ba ratio between 0.5 and 1. Standards and GEOTRACES reference samples (GS & GD, distributed from the 2008 GEOTRACES Intercalibration Cruise) were analyzed in every run for reproducibility, which was within < 2% RSD (Table S1).

GN02/3

At Vrije Universiteit Brussel (VUB), a volume of 0.25 ml of sample was pipetted into an acid cleaned 15 mL polyethylene tube and acidified with 0.15 ml concentrated ultra-pure nitric acid to ensure the stability of Ba measurements. This acidified sub-sample was spiked with 0.15 ml of a ^{135}Ba-spike solution yielding a $^{138/135}$Ba ratio between 0.7 and 1 to minimize error propagation (Klinkenberg et al., 1996; Webster, 1960). Subsequently, the sample was diluted 30-fold with 7 ml Milli-Q grade water to reduce salt content to less than 0.2%. Quantities of sample, spike and dilution water were assessed gravimetrically. The same procedure was employed to prepare blanks (Milli-Q grade water) and reference waters: SLRS-5 & SLRS-3 (National Research Council Canada; Ba concentrations = 14.0 ± 0.5 µg L^{-1} and 13.4 ± 0.6 µg L^{-1}, respectively) and 'OMP' seawater (Mediterranean seawater prepared at Observatoire Midi Pyrénées, Toulouse, France; Ba concentration = 10.4 ± 0.2 µg L^{-1}). Isotope ratios were measured by sector-field inductively-coupled plasma mass spectrometry (SF-ICP-MS; Element 2, Thermo Finnigan). Reproducibility of our method is within < 2 % (RSD) as tested on repeat preparation of SLRS-5 (Table S1).

GN04

At the University of University of Alaska, Fairbanks, dissolved Ba was determined as done at the University of Southern Mississippi (see above GN01) with the following changes: The samples were diluted 100-fold with ultra-pure water (rather than 30-fold) and analyzed by ICP-MS (ThermoFisher Element 2). Furthermore, sample spikes target a $^{138/135}$Ba ratio between 1 and 2. Standards and NRC NASS reference samples (NASS-6 and NASS-7, were analyzed in every run for reproducibility, which was within < 2% RSD (Table S1).

Table S1. Reproducibility and reference standards for dBa and δ^{138}Ba.

Lab	Parameter	Standard	Referenced value	Measured value	RSD %	n	Detection limit
VUB	dBa	SLRS 5 (ppm)	14.0 +/- 0.5	14.02 +/- 0.21	1.53	15	4.7 nM
VUB	dBa	SLRS 3 (ppm)	13.4 +/- 0.6	13.25 +/- 0.33	2.49	15	7.2 nM
VUB	dBa	OMP (ppm)	10.4 +/- 0.2	10.43 +/- 0.24	2.30	7	5.3 nM
USM	dBa	GS (nmol/kg)		44.3 +/- 0.8	1.80	12	2.4 nmol/kg
USM	dBa	GD (nmol/kg)		54.1 +/- 0.9	1.70	12	2.7 nmol/kg
UAF	dBa	NASS-6 (nM)		48.1 +/- 0.8	1.70	18	1.6 nM
UAF	dBa	NASS-7 (nM)		33.1 +/- 0.7	1.43	14	2.1 nM
WHOI	dBa	GSP (nM)		35.4 +/- 0.8		5	
WHOI	dBa	GSC (nM)		41.8 +/- 0.9		8	
WHOI	dBa	D1 (nM)		101.1 +/- 2.0		13	
WHOI	δ^{138}Ba	GSP (‰)		0.61 +/- 0.04		5	
WHOI	δ^{138}Ba	GSC (‰)		0.54 +/- 0.04		8	
WHOI	δ^{138}Ba	D1 (‰)		0.33 +/- 0.03		13	

Text S2. Additional Analytical Protocols for dissolved δ^{138}Ba (GN01)

Sample solutions were aspirated at 140 uL/min with ~1 L/min Ar through a PFA micro-concentric nebulizer (Elemental Scientific) and desolvated in an Aridus II (CETAC). The resultant aerosol was introduced into the MC-ICP-MS and admixed with 3—5 mL/min N_2 to reduce BaO^+ formation (Miyazaki et al., 2014). Analyses were performed in static mode by simultaneously monitoring baseline-corrected ion currents corresponding to *m/z* 131 (Xe; L3), 135 (Ba; L1), 136 (Xe, Ba, Ce; center cup), 137 (Ba; H1), 138 (Ba, Ce, La; H2), 139 (La; H3), and 140 (Ce; H4) for 30 integrations, each ~4.2 s in duration. (Detector baselines were measured by deflecting the ion beam and measuring intensities for 30 s prior to each analysis.) Data reduction was performed using the three-dimensional geometric interpretation of the double spike problem (Siebert et al., 2001) whereby 138/135, 137/135, and 136/135 correspond to the x-, y-, and z-axes, respectively. Sample isotopic composition was solved iteratively—with additional nested loops for isobaric corrections—and reported relative to the nearest four bracketing measurements of NIST

standard reference material 3104a in the delta-notation:

$$\delta^{138}Ba_{NIST}\ (‰) = \left(\frac{\frac{^{138}}{^{134}}Ba_{sample}}{\frac{^{138}}{^{134}}Ba_{NIST}} - 1\right) \times 1000 \qquad \text{(Eqn. 1)}$$

Text S2. Additional Sampling and Analytical Protocols for pBa

GN01

Large and small fraction (> 51 µm & 1 - 51 µm) particulate barium (pBa) samples were collected via McLane Research in situ pumps (WTS-LV) during the GN01 section (following Cutter et al., 2014). This paper reported total pBa (the sum of both large and small fractions). Original data are available at BCO-DMO (Lam, 2020). Pump casts were set up as described in Xiang & Lam (2020). Briefly, filter holders on the McLane pumps were prepared for two flow paths (quartz fiber "QMA" and polyethersulfone "Supor" flow paths) with 142 mm-diameter filter holders. Each path housed a "pre-filter" (51 µm polyester mesh; Sefar 07-51/33). Following the prefilter, the "QMA" path had paired 1.0 µm quartz fiber filters (Whatman QMA) that had been pre-combusted at 450°C for 4 hours. The "Supor" path had paired 0.8 µm polyethersulfone (Pall Supor800) filters. At basin stations (GN01), dBa was collected from the clean rosette which conducted two casts with a total of 23 depths (one overlapping depth). Particulate samples were typically collected from two pump casts for a total of 16 depths; at three stations, three casts were conducted for a total of 24 depths. In comparing the dBa to pBa, sample depths are often not a match.

Particulate barium concentrations were obtained via a refluxing digestion method (Cullen & Sherrell, 1999; Ohnemus et al., 2014; Planquette & Sherrell, 2012). Briefly, the filter was placed onto the wall of a 15 mL flat-bottom screw-cap Savillex vial to avoid immersion. The digestion includes a 4-h refluxing at 110 ˚C with an ultrapure (ARISTAR® or $Optima^{TM}$ grade) 50% HNO_3/10% HF (v/v) mixture and drying down of the acid mixture. By ICP-MS (Thermo Scientific Element XR) at the UCSC Plasma Analytical Facility, final pBa sample solutions were analyzed in low resolution in low resolution. Indium (1 ppb) was used as an internal standard for ICP-MS analysis.

GN02/3

Detailed description of sampling and analysis are presented in Li (2017). Briefly, samples of particulate trace elements were collected from GO-FLO Bottles mounted on a trace metal clean rosette system. At all five stations, samples were collected between between 10 m and near bottom depth. Upon recovery, ~10 L of seawater were collected into LDPE cubitainers and was then filtered through a 0.45 µm Supor filter (47 mm diameter). The filters were subsequently dried, folded in half, and stored in clean poly bags until further analysis. Spaces, containers, and apparatuses were cleaned according to GEOTRACES protocols (Cutter et al., 2014).

Digestion of the particle samples was conducted at the University of British Columbia in a HEPA-filtered fume hood within a class 100 cleanroom. Filters were digested following the Piranha method (Ohnemus et al., 2014). Filters were placed in 15 mL Teflon vials (Savillex) and digested using a mixture of concentrated H_2SO_4 and concentrated H_2O_2 (1.2 mL and 0.4 mL, respectively) at high heat, to digest organic matter and filter matrix. For total digestion, 0.4 mL of concentrated H_2O_2 was added five times with a two hour reflux and slight drying between additions. Following refluxing, samples were dried, washed with 0.1 mL of 8N HNO_3, and dried again. The remaining materials were digested using a concentrated acid mixture of HNO_3:HCl:HF (i.e., 453 µL H_2O, 506 µL HNO_3, 687 µL HCl and 354 µL HF) at 110°C for 4 h. After complete drying, 1 mL of concentrated HNO_3 and 1 mL of concentrated H_2O_2 were added to the vials and taken to dryness again. Following this step, if the digest was yellow, which was uncommon, remaining organic matter was suspected, and another 1 mL of concentrated HNO_3 and 1 mL of concentrated H_2O_2 were added, refluxed, and dried. To the ideal pellet, 0.1 mL of concentrated HNO_3 was added and taken to dryness.

For analysis by ICP-MS (Element2, Thermo Scientific), the final digest was re-suspended in 1% HNO_3 with 10 ppb Indium, as an internal standard. Instrumental blanks were monitored every 6 samples by measuring 1% HNO_3 with Indium. Detection limits and blanks are reported in Li (2017).

GN04

Suspended particles were sampled from the Dutch "ultraclean CTD" sampling system, Titan (de Baar et al., 2008), which consisted of 24 ultra-trace-metal clean polypropylene samplers of 24L each mounted on an all titanium frame with a SEABIRD 911 CTD system and deployed on a 11 mm Dyneema cable. After recovery, the complete "ultraclean CTD" was immediately placed in an ISO Class 6 clean room container, where samples for particulate trace elements were collected on 25mm diameter 0.45 µm polyethersulfone filters (Pall Supor) mounted in swinnex filter holders under pressure of filtered N2 (0.7 bar) applied via the top-connector of the polypropylene sampler. Between 4 and 10L were filtered through the filters.

Particulate barium concentrations were obtained via a refluxing digestion method (Planquette & Sherrell, 2012). Briefly, the filter was placed onto the wall of a 15 mL flat-bottom screw-cap Savillex vial to avoid immersion. The digestion includes a 4-h refluxing at 110 ˚C with an ultrapure (Merck) 50% HNO3/10% HF (v/v) mixture and drying down of the acid mixture. Residues were re-dissolved using a 3% HNO3 (v/v) solution then analyzed by SF-ICP-MS (Thermo Scientific Element XR) at the Pôle Spectrometrie Océans (France) in low resolution. Indium (1 ppb) was used as a drift monitor.

Text S3. Intercalibration of GEOTRACES Crossover Stations

The suite of cruises was conducted such that crossover stations, whereby two cruises

occupied the same station, could occur (Figure S1). We report the locations of each crossover station in Table S2. Generally, the stations compare well and there are acceptably low offsets (Figure S2a). For dissolved Ba, calibration offsets > 2.5 are only observed in the upper 500 m of the water column where there is the influence of a strong halocline. Thus, in the upper 500 m of the water column small differences in depth may result in large changes in dBa. Similarly to dBa, pBa may also be influenced by the halocline and pBa offsets > 50 pM are only observed in the upper 500 m of the water column.

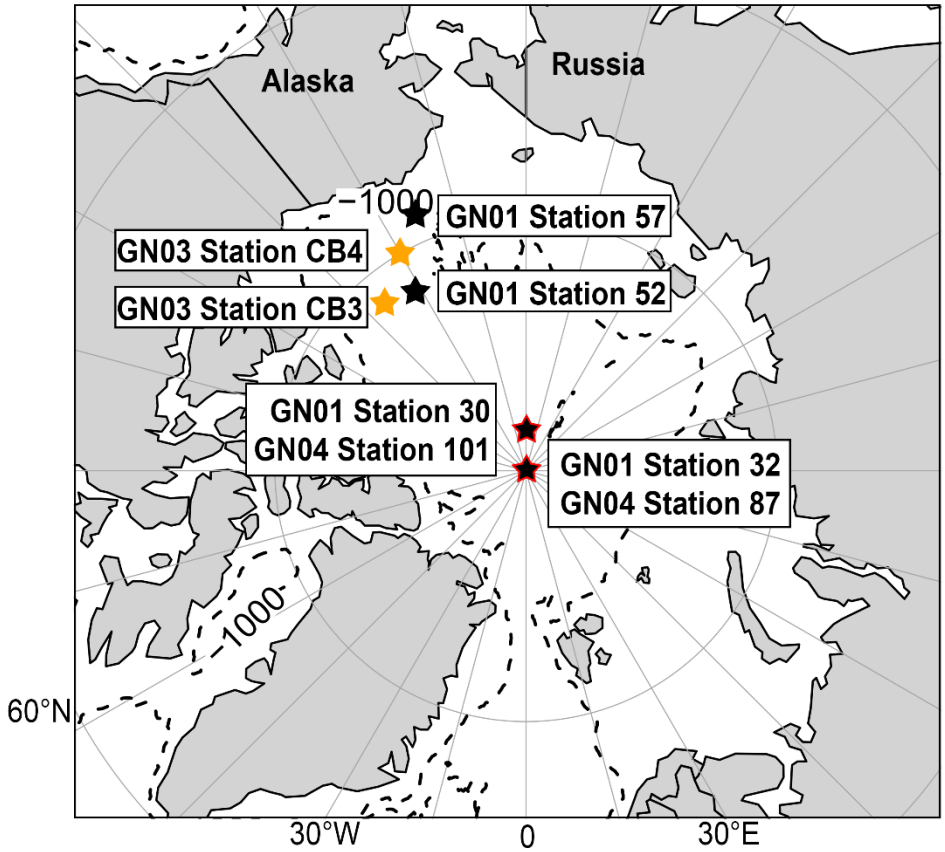

Figure S1. Cross-over station conducted in three separate 2015 Arctic GEOTRACES cruises. Black colors indicate US stations, red colors indicate European stations, and orange indicates Canadian stations.

Table S2. Intercalibration exercise between cruises.

Cruise	Station	Latitude (°N)	Longitude (°E)	Approximate Distance between stations (km)	Dissolved Ba (nmol kg^{-1})			Particulate Ba (pmol L^{-1})		
					Median Offset	Min Offset	Max Offset	Median Offset	Min Offset	Max Offset
GN01	32	89.99	32.54	7	0.63	0.24	1.84	49.2	21.5	96.9
GN04	87	89.93	-120.19							
GN01	30	87.52	-179.81	3	2.01	0.20	8.10	19.2	0.6	188.1
GN04	101	87.50	179.80							
GN01	57	73.39	-156.53	266	1.94	0.12	18.07	33.8	13.8	82.6
GN02/3	CB4	75.00	-150.00							
GN01	52	77.50	-148.01	203	1.10	0.14	10.76	31.9	10.5	161.2
GN02/3	CB3	76.99	-140.05							
Summary					**1.40**	**0.12**	**18.07**	**31.5**	**0.6**	**188.1**

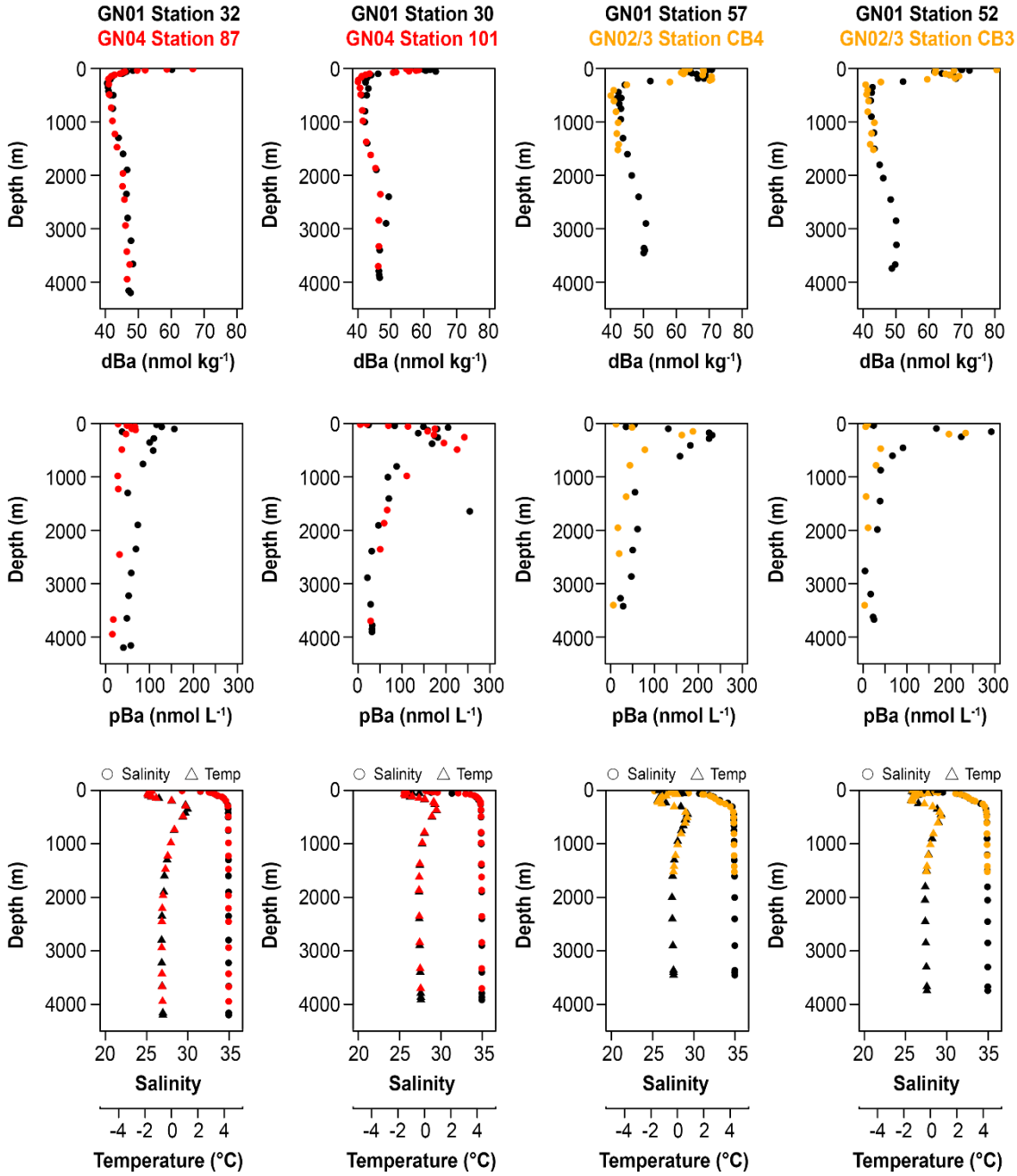

Figure S2. Cross-over station comparison. Following GEOTRACES Standards for intercalibration we compare for dBa (top row) and pBa (middle row) between stations conducted at roughly the same location on between cruises. The bottom row references temperature and salinity profiles for each station.

Text S4. Comparison of dBa and pBa to the North Pacific and North Atlantic Oceans

The distribution of dissolved and particulate Ba in the western Arctic Ocean is unique compared to vertical distributions in the North Pacific and North Atlantic Oceans

(Figure S3). Dissolved Ba distributions in the North Pacific and Atlantic follow a nutrient-like profile shape: low in the surface and generally increasing with depth. In the western Arctic Ocean basins, dBa is highest in the surface waters (< 300 m) and decreases between 300 and 2000 m depth before increasing toward the bottom.

Particulate Ba usually has a mesopelagic maximum; in the western Arctic Ocean the maximum is slightly shallower than in other ocean basins.

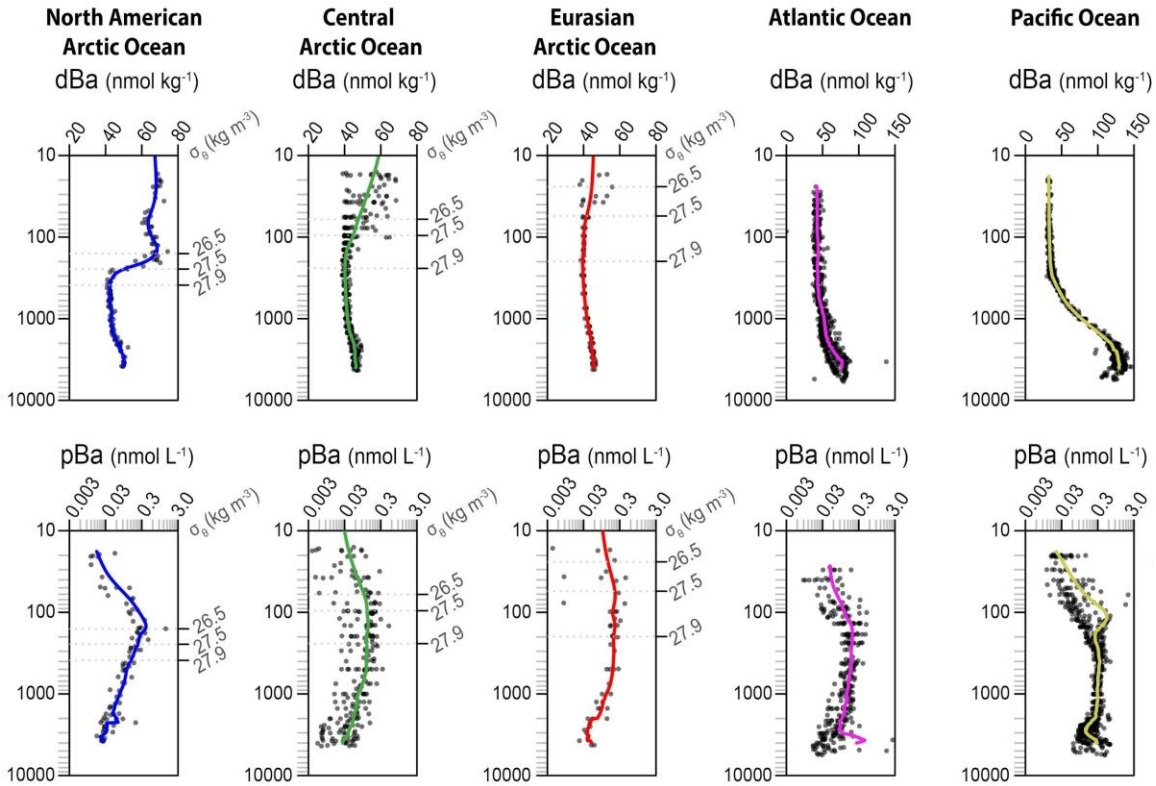

Figure S3. Comparison of Arctic Ocean dBa and pBa vertical distributions to the Pacific Ocean (GP16) and Atlantic Ocean (GA03). Data for the Atlantic and Pacific Oceans was extracted from the GEOTRACES Intermediate Data Product (Version 2) (Schlitzer et al., 2018).

Text S5. The Flux Balance Approach to the dissolved Ba Budget

The box we consider in our elemental budget is the upper 500 m of the Arctic Ocean water column where bottom depths are greater than 1000 m (Figure S4). Two datasets are used separately to consider how the balance has changed since the early measurements of dBa in the Arctic Ocean: the 2015 Arctic GEOTRACES data and the 1994 Arctic Ocean Survey.

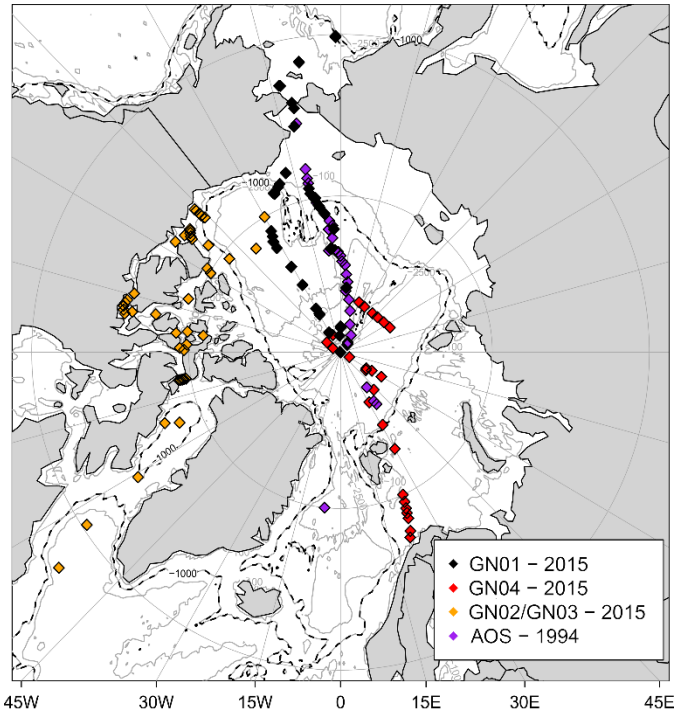

Figure S4. The spatial outer bounds of the box model are roughly identified in this figure. The 1000 m isobath is identified by the dashed line, the model is informed by all data points north of the Bering Strait, Fram Strait, and Canadian Arctic Archipelago (i.e., the Arctic Ocean Basins). Two scenarios were run using data from the 2015 GEOTRACES surveys and from the 1994 AOS survey.

Text S6. Comparison of the box model results to Ra-flux predicted Ba fluxes

In the manuscript text we describe the results of our box model; which indicated that approximately 50% of the dBa budget is sourced from the shelves. Here, we use the dBa:Ra relationship on the shelf to predict the fluxes of dBa from shelf sediments such that: $\boldsymbol{F_{Ba}} = \frac{\boldsymbol{dBa}}{\boldsymbol{dRa}} \times \boldsymbol{F_{Ra}}$. Where F indicates flux (with the superscript representing the element) and dBa and dRa indicating the ratio of those elements on the shelves. The flux of radium (F_{Ra} in atoms/y) was directly from Kipp et al. (2018). We determined the dBa:dRa ratio using shelf dBa (nmol/L) data from this study and shelf ^{228}Ra data from Kipp et al. (2018). The ratio used is the regression of the two parameters (Figure S5).

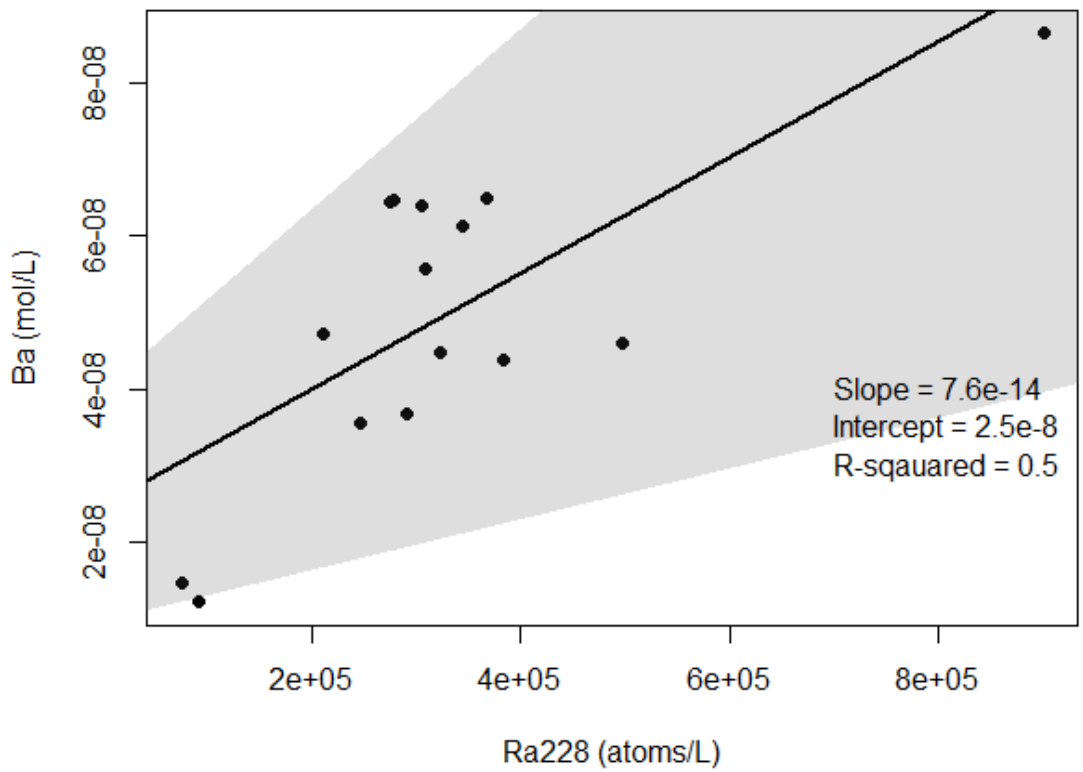

Figure S5. The observed relationship between dBa and dissolved ^{228}Ra. Data points are from the western Arctic shelves (Bering and Chukchi Sea) sampled during the 2015 GN01 expedition. The black line is a type II linear regression and the gray shaded area is the 95% confidence interval.

Text S7. Evidence of hydrothermal Ba in the Eurasian Arctic

Two stations in the GN04 transect sit near the Nansen-Gakkel Ridge Crest. One station has dissolved distributions of dBa that reflect hydrothermal input (i.e., deep water maxima between 2000 and 3000 m; Figure S6).

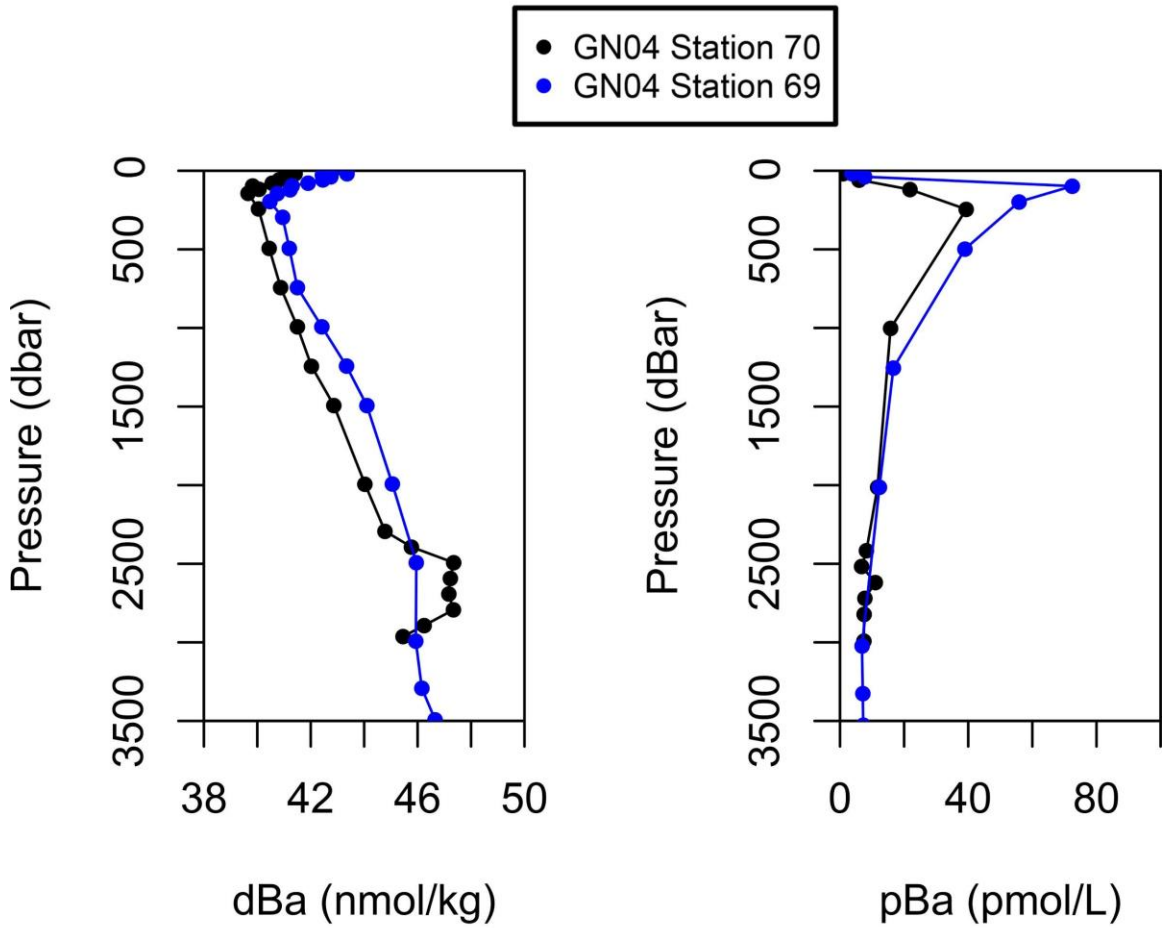

Figure S6. Nansen-Gakkel Ridge Crest Stations. The black dots and lines represent station 70, which appears to be influenced by a dBa source between 2000 and 3000 dbar (hydrothermal input); there also may be a slight input of pBa to the water column. Blue lines are the nearby station 69; which does not appear to be influenced by the hydrothermal plume.

Text S8. Dissolved Ba Salinity Relationships in the Canadian Arctic Archipelago

We investigated the dBa-Salinity relationships to probe how rivers or sea ice melt might influence dBa concentrations. Broadly through the Archipelago there are two salinity patterns. At high salinities (S > 32.5), dBa decreases with increasing S. This is consistent with mixing of Atlantic-source water with Pacific-origin waters in the Arctic Ocean basins. However, we note that there is a large amount of scatter in the CAA trend, which is not observed in the Arctic Ocean. At low salinities (S < 32.5) dBa decreases slightly, which is roughly in line with how a slight contribution of sea ice would dilute the seawater concentrations. We suspect there is not a large river influence as at low salinities (S < 32.5), dBa decreases; generally, rivers have high dBa signatures and would drive dBa up at low salinity. We note that the concentrations of dBa in CAA rivers is not well constrained, but studies show a broad range of possible endmember (Colombo et al.,

2019). Most of the possible endmembers are higher than seawater, but a few do fall below the seawater concentration. Thus, it is possible there is slight river influence in addition to sea ice melt at the low salinity range.

Here, we diagnose the reason for the scatter at the high salinity range by looking at stations in the CAA (Parry Channel) moving from the Arctic Ocean eastward to Lancaster Sound. We follow the dBa at each station and highlight the dBa at S = 32.5, the salinity of Pacific-derived seawater. Moving eastward, dBa at S = 32.5 decreases, furthermore, the dBa on the north side of the channel (CAA4 and CAA6) can be substantially lower than on the south side of the channel (CAA5 and CAA7). We note that CAA7 is tucked just south of the Parry Channel, in a northward flowing channel of the Archipelago. Due to its position, it may not be perfectly representative of waters flowing from the Arctic through Parry Channel. On the south side of the Parry Channel, dBa decreased to ~56 nmol/kg at S = 32.5 (from ~65 nmol/kg in the Canada Basin and western extent of Parry channel). On the north side of the channel, dBa reached as low as 50 nmol/kg at S = 32.5. We suggest this erosion of the high dBa signal is due to mixing of Atlantic-like waters in Baffin Bay with the eastern extent of the Parry Channel.

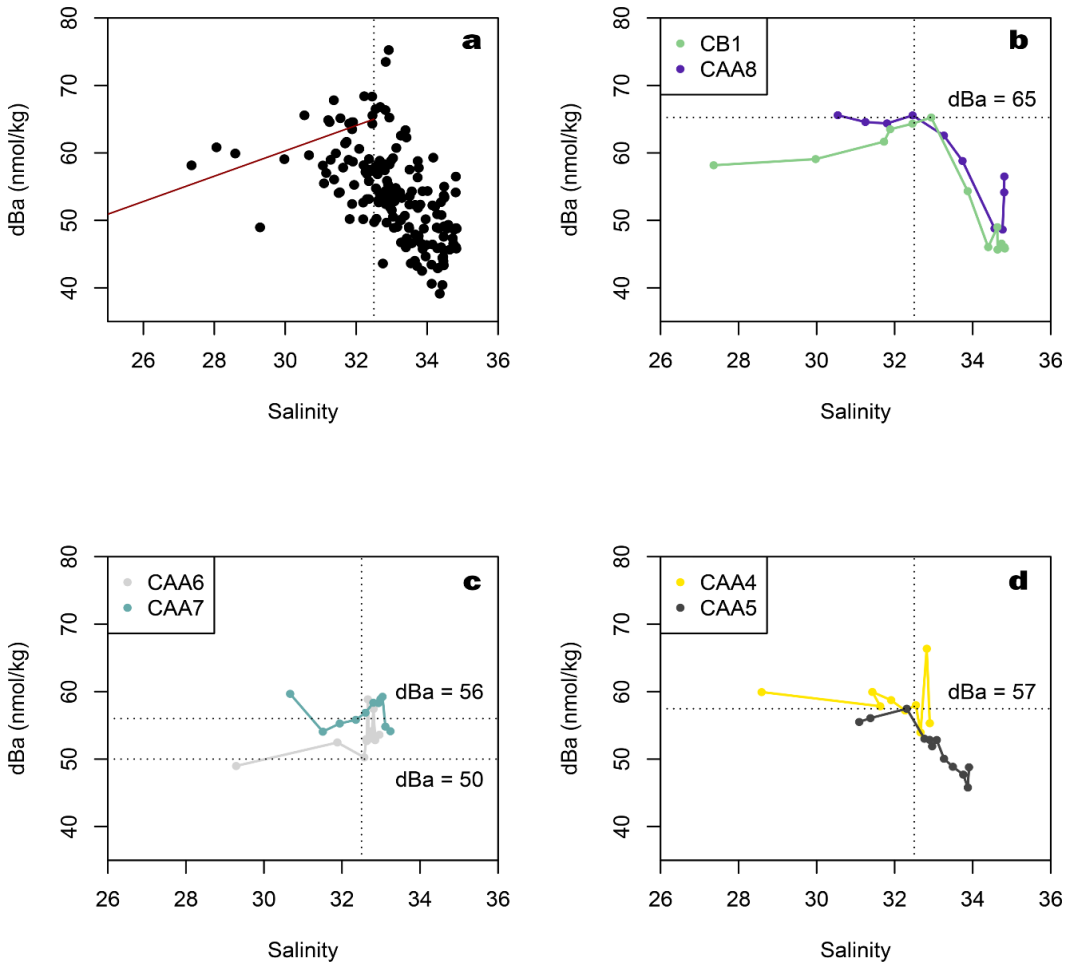

Figure S7. dBa-Salinity patterns in the CAA. In all panels the dashed vertical line is S = 32.5 and is representative of Pacific-derived seawater; the dashed horizontal line is the dBa at S = 32.5. a) all stations and samples in the Parry Channel. The red line denotes mixing with sea ice melt. b) Stations on the Arctic Ocean (western) side of the Parry Channel; CB1 is in the Canada Basin and CAA8 is in the Parry Channel. Both of these stations have a "western Arctic Ocean-like" signal, where Pacific-derived seawater is high in dBa (~65 nmol/kg). c) Stations CAA6 and CAA7 (just west of the Barrow Strait in Parry Channel). Dissolved Ba has decreased to 56 nmol/kg on the south side of the Channel and 50 nmol/kg on the north side of the channel. d) Stations CAA4 (north side of channel) and CAA5 (south side of channel) are located just east of the Barrow Strait. They have roughly equivalent dBa (57 nmol/kg).

References

Colombo, M., Brown, K. A., De Vera, J., Bergquist, B. A., & Orians, K. J. (2019). Trace metal geochemistry of remote rivers in the Canadian Arctic Archipelago. *Chemical Geology*, *525*, 479–491. https://doi.org/10.1016/j.chemgeo.2019.08.006

Cullen, J. T., & Sherrell, R. M. (1999). Techniques for determination of trace metals in small samples of size-fractionated particulate matter: phytoplankton metals off central California. *Marine Chemistry*, *67*(3–4), 233–247. https://doi.org/10.1016/S0304-4203(99)00060-2

Cutter, G., Andersson, P. S., Codispoti, L. A., Croot, P., Francois, R., Lohan, M., et al. (2014). Sampling and Sample-handling Protocols for GEOTRACES Cruises, *Version 2*. http://www.geotraces.org/library-88/scientific-publications/reports/169-sampling-and-sample-handling-protocols-for-geotraces-cruises

De Baar, H. J. W., Timmermans, K. R., Laan, P., De Porto, H. H., Ober, S., Blom, J. J., et al. (2008). Titan: A new facility for ultraclean sampling of trace elements and isotopes in the deep oceans in the international Geotraces program. *Marine Chemistry*, *111*(1–2), 4–21. https://doi.org/10.1016/j.marchem.2007.07.009

Kipp, L. E., Charette, M. A., Moore, W. S., Henderson, P. B., & Rigor, I. G. (2018). Increased fluxes of shelf-derived materials to the central Arctic Ocean. *Science Advances*, *4*(1), eaao1302. https://doi.org/10.1126/sciadv.aao1302

Klinkenberg, H., Van Borm, W., & Souren, F. (1996). A theoretical adaptation of the classical isotope dilution technique for practical routine analytical determinations by means of inductively coupled plasma mass spectrometry. *Spectrochimica Acta Part B: Atomic Spectroscopy*, *51*(1), 139–153. https://doi.org/10.1016/0584-8547(95)01386-5

Klinkhammer, G. P., & Chan, L. H. (1990). Determination of barium in marine waters by isotope dilution inductively coupled plasma mass spectrometry. *Analytica Chimica Acta*, *232*, 323–329.

Lam, P. (2020). Size-fractionated major and minor particle composition and concentration from the US GEOTRACES Arctic cruise (HLY1502) on USCGC Healy from August to October 2015. (Version (Version 1) Version Date 2020-04-01). Biological and Chemical Oceanographic Data Management Office (BCO-DMO).

Li, J. (2017). *Particulate Trace Metals & Iron Availability to Phytoplankton in a Changing Arctic Ocean* (Masters of Science). University of British Columbia.

Ohnemus, D. C., Auro, M. E., Sherrell, R. M., Lagerström, M., Morton, P. L., Twining, B. S., et al. (2014). Laboratory intercomparison of marine particulate digestions including Piranha: a novel chemical method for dissolution of polyethersulfone filters. *Limnology and Oceanography: Methods*, *12*(8), 530–547. https://doi.org/10.4319/lom.2014.12.530

Planquette, H., & Sherrell, R. M. (2012). Sampling for particulate trace element determination using water sampling bottles: methodology and comparison to in situ pumps: Particulate trace element sampling. *Limnology and Oceanography: Methods*, *10*(5), 367–388. https://doi.org/10.4319/lom.2012.10.367

Schlitzer, R., Anderson, R. F., & Masferrer Dodas, E. (2018). The GEOTRACES Intermediate Data Product 2017. *Chemical Geology*.

https://doi.org/10.1016/J.CHEMGEO.2018.05.040
Siebert, C., Nägler, T. F., & Kramers, J. D. (2001). Determination of molybdenum isotope fractionation by double-spike multicollector inductively coupled plasma mass spectrometry. *Geochemistry, Geophysics, Geosystems*, *2*(7), 2000GC00124. https://doi.org/10.1029/2000GC000124
Webster, R. K. (1960). Mass spectrometric isotope dilution analysis. In *Methods in geochemistry* (pp. 202–246). London: Interscience.
Xiang, Y., & Lam, P. J. (2020). Size-fractionated marine suspended particle dynamics in the Western Arctic Ocean: Lateral and vertical sources. *Journal of Geophysical Research: Oceans*, *125*(8), e2020JC016144.